Hindawi Publishing Corporation
ISRN Mathematical Physics
Volume 2013, Article ID 748613, 24 pages
http://dx.doi.org/10.1155/2013/748613

Research Article

Air-Aided Shear on a Thin Film Subjected to a Transverse Magnetic Field of Constant Strength: Stability and Dynamics

Mohammed Rizwan Sadiq Iqbal

Department of Mathematics and Statistics, University of Constance, 78457 Constance, Germany

Correspondence should be addressed to Mohammed Rizwan Sadiq Iqbal; rizwan.sadiq.i@gmail.com

Received 28 June 2013; Accepted 22 August 2013

Academic Editors: L. E. Oxman and W.-H. Steeb

The effect of air shear on the hydromagnetic instability is studied through (i) linear stability, (ii) weakly nonlinear theory, (iii) sideband stability of the filtered wave, and (iv) numerical integration of the nonlinear equation. Additionally, a discussion on the equilibria of a truncated bimodal dynamical system is performed. While the linear and weakly nonlinear analyses demonstrate the stabilizing (destabilizing) tendency of the uphill (downhill) shear, the numerics confirm the stability predictions. They show that (a) the downhill shear destabilizes the flow, (b) the time taken for the amplitudes corresponding to the uphill shear to be dominated by the one corresponding to the zero shear increases with magnetic fields strength, and (c) among the uphill shear-induced flows, it takes a long time for the wave amplitude corresponding to small shear values to become smaller than the one corresponding to large shear values when the magnetic field intensity increases. Simulations show that the streamwise and transverse velocities increase when the downhill shear acts in favor of inertial force to destabilize the flow mechanism. However, the uphill shear acts oppositely. It supports the hydrostatic pressure and magnetic field in enhancing films stability. Consequently, reduced constant flow rates and uniform velocities are observed.

1. Introduction

A nonlinear fourth-order degenerate parabolic differential equation of the form:

$$h_t + \mathscr{A}(h)\, h_x + \frac{\partial}{\partial x}\left\{\mathscr{B}(h)\, h_x + \mathscr{C}(h)\, h_{xxx}\right\} = 0, \qquad (1)$$

where $\mathscr{A}$, $\mathscr{B}$, and $\mathscr{C}$ are arbitrary continuous functions of the interfacial thickness $h(x,t)$, represents a scalar conservation law associated to the flow of a thin viscous layer on an incline under different conditions. The stability and dynamics of equations of the type of (1) is a subject of major interest [1–18] because of their robustness in regimes where viscosity dominates inertia [19]. Such studies have focused attention primarily on the isothermal and nonisothermal instability analysis, mainly for nonconducting fluids.

Since the investigation of Chandrasekar [20] on the stability of a flow between coaxial rotating cylinders in the presence of a magnetic field held in the axial direction, the laminar flow of an electrically conducting fluid under the presence of a magnetic field has been studied extensively. For instance, Stuart [21] has reported on the stability of a pressure flow between parallel plates under the application of a parallel magnetic field. Among other earlier investigations, Lock [22] examined the stability when the magnetic field is applied perpendicular to the flow direction and to the boundary planes. Hsieh [23] found that the magnetic field stabilizes the flow through Hartmann number when the electrically conducting fluid is exposed to a transverse magnetic field, provided that the surface-tension effects are negligible in a horizontal film. Ladikov [24] studied a problem in the presence of longitudinal and transverse magnetic fields. The author observed that the longitudinal magnetic field plays a stabilizing role and that the effect of instability at small wave numbers could be removed if the longitudinal magnetic field satisfies certain conditions. Lu and Sarma [25] investigated the transverse effects of the magnetic field in magnetohydrodynamic gravity-capillary waves. The flow of an electrically conducting fluid over a horizontal plane in the presence of tangential electric and magnetic fields was

reported by Gordeev and Murzenko [26]. They found that the flow suffers from instability not due to the Reynolds number but due to the strength of the external electric field.

In applications such as magnetic-field-controlled material-processing systems, aeronautics, plasma engineering, MEMS technology, and magnetorheological lubrication technologies, the hydromagnetic effects are important. Also, liquid metal film flows are used to protect the solid structures from thermonuclear plasma in magnetic confinement fusion reactors, and this application requires a better understanding of the instability mechanism arising in a thin magnetohydrodynamic flow over planar substrates [27]. Furthermore, the presence of an external magnetic field regulates the thickness of a coating film. It prevents any form of direct electrical or mechanical contact with the fluid thereby reducing the risk of contamination [28]. Renardy and Sun [29] pointed out that the magnetic fluid is effective in controlling the flow of ordinary fluids and in reducing hydraulic resistance. The reason is that the magnetic fluids can be easily controlled with external magnetic fields and that coating streamlined bodies with a layer of less-viscous magnetic fluid significantly reduces the shear stress in flow boundaries. Magnetohydrodynamic flow can be a viable option for transporting weakly conducting fluids in microscale systems such as flows inside a micro-channel network of a lab-on-a-chip device [30, 31]. In all of the above applications, considering the associated stability problem is important because it gives guidance in choosing the flow parameters for practical purposes. In this regard, in the past two decades, the emerging studies on the hydromagnetic effects have focused their attention on stability problems and on analyzing the flow characteristics [28, 29, 32–43].

The shearing effect of the surrounding air on the fluid in realistic situations induces stress tangentially on the interfacial surface. The hydrodynamic instability in thin films in the presence of an external air stream attracted attention in the mid 1960s, which led Craik [44] to conduct laboratory research and study theory. He found that the instability occurs regardless of the magnitude of the air stream when the film is sufficiently thin. Tuck and Vanden-Broeck [45] reported on the effect of air stream in industrial applications of thin films of infinite extent in coating technology. Sheintuch and Dukler [46] did phase plane and bifurcation analyses of thin wavy films subjected to shear from countercurrent gas flows and found satisfactory agreement of their results connected to the wave velocity along the flooding curve with the experimental results of Zabaras [47]. Although the experimental results related to the substrate thickness did not match exactly with the theoretical predictions, still the results gave qualitative information about the model. Thin liquid layer supported by steady air-flow surface-traction was reported by King and Tuck [48]. Their study models the surface-traction-supported fluid drops observed on the windscreen of a moving car on a rainy day. Incorporating the superficial shear offered by the air, Pascal [49] studied a problem which models the mechanism of wind-aided spreading of oil on the sea and found quantitative information regarding the maximum upwind spread of the gravity current. Wilson and Duffy [50] studied the steady unidirectional flow of a thin rivulet on a vertical substrate subjected to a prescribed uniform longitudinal shear stress on the free surface. They categorized the possible flow patterns and found that the direction of the prescribed shear stress affects the velocity in the entire rivulet. The generation of roll waves on the free boundary of a non-Newtonian liquid was numerically assessed using a finite volume method by Pascal and D'Alessio [51], revealing the significant effect of air shear on the evolution of the flow. Their study showed that the instability criteria was conditional and depends on the directionally induced shear. Kalpathy et al. [52] investigated an idealized model suitable for lithographic printing by examining the shear-induced suppression of two stratified thin liquid films confined between parallel plates taking into account the van der Waals force. A film thickness equation for the liquid-liquid interface was derived in their study using lubrication approximation. They found that the effect of shear affects the imaginary part of the growth rate, indicating the existence of traveling waves. Furthermore, they also observed a critical shear rate value beyond which the rupture mechanism could be suppressed. This study motivated Davis et al. [53] to consider the effect of unidirectional air shear on a single fluid layer. For a two-dimensional ultrathin liquid, Davis et al. [53] showed that the rupture mechanism induced by the London van der Waals force could be suppressed when the magnitude of the wind shear exceeds a critical value, as observed by Kalpathy et al. [52]. Recently, Uma [18] measured numerically the profound effect of unidirectional wind stress on the stability of a condensate/evaporating power-law liquid flowing down an incline.

In the present investigation, the effects of downhill and uphill air shear on a thin falling film in the presence of a transverse magnetic field are studied. Such an investigation will illustrate the realistic influence of the natural environment acting upon the flows. Or, it may illustrate the need to control the flow mechanism through artificial techniques, which blow air when the hydromagnetic effects are considered. The outline of this paper is organized as follows. Section 1 presents the introduction. In Section 2, mathematical equations governing the physical problem are presented. Section 3 discusses the long-wave Benney-type equation. In Section 4, linear stability analysis, weakly nonlinear stability analysis, and the instability arising due to sideband disturbances are analyzed. The equilibria of a truncated bimodal dynamical system is mathematically presented in Section 5. While the results in Section 6 discuss nonlinear simulations of the film thickness evolution, Section 7 highlights the main conclusions of the study and includes future perspectives.

2. Problem Description

A thin Newtonian liquid layer of an infinite extent falling freely over a plane under the influence of gravitational acceleration, g, is considered. The flow is oriented towards the x-axis, and the plane makes an angle β with the horizon. Properties of the fluid like density (ρ), viscosity (μ), and surface-tension (σ) are constants. The magnetic flux density is defined by the vector $\mathbf{B} = B_0 \vec{j}$, where B_0 is the magnitude of

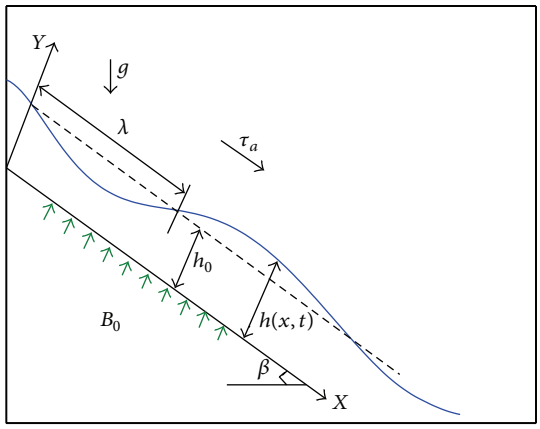

Figure 1: Sketch of the flow configuration. When $\tau_a > 0$, the air shears the surface along the downhill direction (in the direction of the arrow). However, if $\tau_a < 0$, the air shears the surface along the uphill direction (in this case, the arrow would point to the opposite direction). The air shear effect is zero when $\tau_a = 0$.

the magnetic field imposed along the y-direction (Figure 1). It is assumed that there is no exchange of heat between the liquid and the surrounding air, but an air flow (either in the uphill or in the downhill direction) induces a constant stress of magnitude τ_a on the interface and moves tangentially along the surface. The y-axis is perpendicular to the planar substrate such that, at any instant of time t, $h(x,t)$ measures the film thickness.

The magnetohydrodynamic phenomena can be modeled by the following equations, which express the momentum and mass balance:

$$\rho\left(\frac{\partial \mathbf{U}}{\partial t} + \mathbf{U}\cdot\nabla\mathbf{U}\right) = \rho\mathbf{G} - \nabla p + \mu\nabla^2\mathbf{U} + \mathbf{F}, \tag{2}$$

$$\nabla\cdot\mathbf{U} = 0. \tag{3}$$

The last term in (2) arises due to the contribution of Lorenz body force, based on Maxwell's generalized electromagnetic field equations [28, 54, 55].

In a realistic situation corresponding to a three-dimensional flow, the total current flow can be defined using Ohm's law as follows:

$$\mathbf{J} = \Sigma\left(\mathbf{E} + \mathbf{U}\times\mathbf{B}\right), \tag{4}$$

where $\mathbf{J}$, $\mathbf{E}$, $\mathbf{U}$, and Σ represent the current density, electric field, velocity vector, and electrical conductivity, respectively. The Lorenz force acting on the liquid is defined as $\mathbf{F} = \mathbf{J}\times\mathbf{B}$. In the rest of the analysis, a short circuited system corresponding to a two-dimensional problem is considered by assuming that $\mathbf{E} = 0$. This assumption simplifies the last term corresponding to the electromagnetic contribution in (2). In this case, the pondermotive force acting on the flow (the last term in (2)) has only one nonvanishing term in the x-direction; therefore,

$$\mathbf{F} = \left(F_x, F_y\right) = \left(-\Sigma B_0^2 u, 0\right), \tag{5}$$

where $\mathbf{G} = (g\cos\beta, -g\sin\beta)$ and p is the pressure.

Boundary conditions on the planar surface and the interface are added to complete the problem definition of (2)-(3). On the solid substrate, the no-slip and the no-penetration conditions are imposed, which read as

$$\mathbf{U} = (u, v) = 0. \tag{6}$$

The jump in the normal component of the surface-traction across the interface is balanced by the capillary pressure (product of the mean surface-tension coefficient and the local curvature of the interface), which is expressed as

$$\begin{aligned} p_a - p + \left(\mu\left(\nabla\mathbf{U} + \nabla\mathbf{U}^T\right)\cdot\mathbf{n}\right)\cdot\mathbf{n} \\ = 2\sigma\Pi(h) \quad \text{on} \quad y = h(x,t), \end{aligned} \tag{7}$$

where $\Pi(h) = -(1/2)\nabla\cdot\mathbf{n}$ is the mean film curvature and p_a is the pressure afforded by the surrounding air. The unit outward normal vector at any point on the free surface is $\mathbf{n} = \nabla(y-h)/|\nabla(y-h)|$, and $\mathbf{t}$ represents the unit vector along the tangential direction at that point such that $\mathbf{n}\cdot\mathbf{t} = 0$. The tangential component of the surface-traction is influenced by the air stress τ_a and reads as

$$\left(\mu\left(\nabla\mathbf{U} + \nabla\mathbf{U}^T\right)\cdot\mathbf{t}\right)\cdot\mathbf{n} = \tau_a \quad \text{on} \quad y = h(x,t). \tag{8}$$

The location of the interface can be tracked through the following kinematic condition:

$$\frac{\partial h}{\partial t} = v - u\frac{\partial h}{\partial x} \quad \text{on} \quad y = h(x,t). \tag{9}$$

In order to remove the units associated with the model (2)–(9) involving the physical variables, reference scales must be prescribed. In principle, one can nondimensionalize the system based on the nature of the problem by choosing one of the following scales [9, 16]: (a) kinematic viscosity based scales, (b) gravitational acceleration as the flow agent based scales, (c) mean surface-tension based scales, and (d) Marangoni effect as the flow agent based scales. However, for very thin falling films, the main characteristic time is the viscous one [7–9, 16]. An advantage of choosing the viscous scale is that either both the large and the small inclination angles could be considered by maintaining the sine of the angle and the Galileo number as separate entities [7, 16] or the Reynolds number as a product of Galileo number and sine of the inclination angle could be defined as a single entity [9]. Also, such a scale plays a neutral role while comparing the action of gravity and Marangoni effect in nonisothermal problems [16]. Choosing the viscous scale, the horizontal distance is scaled by l, vertical distance by h_0, streamwise velocity by ν/h_0 , transverse velocity by ν/l, pressure by $\rho\nu^2/h_0^2$, time by lh_0/ν, and, finally, the shear stress offered by the wind by $\rho\nu^2/h_0^2$. In addition, the slenderness parameter ($\varepsilon = h_0/l$) is considered small, and a gradient expansion of the dependent variables is done [7–9]. The horizontal length scale, l, is chosen such that $l = \lambda$, where λ is a typical wavelength larger than the film thickness.

The dimensionless system is presented in Appendix A (the same symbols have been used to avoid new notations). The set of nondimensional parameters arising during nondimensionalization procedure are $\mathrm{Re} = \mathrm{Ga}\sin\beta$ (the Reynolds number) [9], $\mathrm{Ga} = gh_0^3/\nu^2$ (the Galileo number), $\mathrm{Ha} = \Sigma B_0^2\, h_0^2/\mu$ (the Hartmann number, which measures the relative importance of the drag force resulting from magnetic induction to the viscous force arising in the flow), $\overline{\mathcal{S}} = \sigma h_0/\rho\nu^2$ (the surface-tension parameter), and $\tau = \tau_a h_0^2/\rho\nu^2$ (the shear stress parameter). The surface-tension parameter is usually large; therefore, it is rescaled as $\varepsilon^2\,\overline{\mathcal{S}} = S$ and set as $\mathcal{O}(1)$ in accordance to the waves observed in laboratory experiments. All of the other quantities are considered $\mathcal{O}(1)$. The long-wave equation is derived in the next step.

3. Long-Wave Equation

The dependent variables are asymptotically expanded in terms of the slenderness parameter ε to derive the long-wave equation. Using the symbolic math toolbox available in MATLAB, the zeroth and the first-order systems are solved. These solutions are then substituted in the kinematic condition (A.5) to derive a Benney-type model accurate up to $\mathcal{O}(\varepsilon)$ of the form (1) as

$$h_t + A(h)\,h_x + \varepsilon\left(B(h)\,h_x + C(h)\,h_{xxx}\right)_x + \mathcal{O}\left(\varepsilon^2\right) = 0. \quad (10)$$

The standard procedure for the derivation [7, 9, 14, 15, 28] is skipped here. The expressions for $A(h)$, $B(h)$, and $C(h)$ are, the following:

$$A(h) = \frac{\mathrm{Re}}{\mathrm{Ha}}\tanh^2\left(\sqrt{\mathrm{Ha}}\,h\right) + \frac{\tau}{\sqrt{\mathrm{Ha}}}\tanh\left(\sqrt{\mathrm{Ha}}\,h\right)\mathrm{sech}\left(\sqrt{\mathrm{Ha}}\,h\right), \quad (11)$$

$$\begin{aligned} B(h) = {} & \left\{\frac{\mathrm{Re}\,\cot\beta}{\mathrm{Ha}^{3/2}}\tanh\left(\sqrt{\mathrm{Ha}}\,h\right) - \frac{\mathrm{Re}\,\cot\beta h}{\mathrm{Ha}}\right\} \\ & + \left\{\frac{\mathrm{Re}^2 h}{2\mathrm{Ha}^{5/2}}\tanh\left(\sqrt{\mathrm{Ha}}\,h\right)\mathrm{sech}^4\left(\sqrt{\mathrm{Ha}}\,h\right)\right. \\ & \quad + \frac{\mathrm{Re}^2 h}{\mathrm{Ha}^{5/2}}\tanh\left(\sqrt{\mathrm{Ha}}\,h\right)\mathrm{sech}^2\left(\sqrt{\mathrm{Ha}}\,h\right) \\ & \quad \left. - \frac{3\mathrm{Re}^2}{2\mathrm{Ha}^3}\tanh^2\left(\sqrt{\mathrm{Ha}}\,h\right)\mathrm{sech}^2\left(\sqrt{\mathrm{Ha}}h\right)\right\} \\ & + \tau\left\{\frac{3\,\mathrm{Re}}{2\mathrm{Ha}^{5/2}}\tanh\left(\sqrt{\mathrm{Ha}}\,h\right)\mathrm{sech}\left(\sqrt{\mathrm{Ha}}\,h\right)\right. \\ & \quad \left. - \frac{3\,\mathrm{Re}}{\mathrm{Ha}^{5/2}}\tanh\left(\sqrt{\mathrm{Ha}}\,h\right)\mathrm{sech}^3\left(\sqrt{\mathrm{Ha}}\,h\right)\right. \\ & \quad + \frac{\mathrm{Re}\,h}{\mathrm{Ha}^2}\left(\mathrm{sech}^5\left(\sqrt{\mathrm{Ha}}\,h\right)\right. \\ & \qquad \left. + \frac{3}{2}\,\mathrm{sech}^3\left(\sqrt{\mathrm{Ha}}\,h\right)\right. \\ & \qquad \left. \left. -\mathrm{sech}\left(\sqrt{\mathrm{Ha}}\,h\right)\right)\right\} \\ & + \tau^2\left\{\frac{h\tanh\left(\sqrt{\mathrm{Ha}}\,h\right)}{\mathrm{Ha}^{3/2}}\left(-\mathrm{sech}^2\left(\sqrt{\mathrm{Ha}}\,h\right)\right.\right. \\ & \qquad \left.\left. -\frac{1}{2}\,\mathrm{sech}^4\left(\sqrt{\mathrm{Ha}}\,h\right)\right)\right. \\ & \quad \left. + \frac{3}{2\mathrm{Ha}^2}\tanh^2\left(\sqrt{\mathrm{Ha}}\right)\mathrm{sech}^2\left(\sqrt{\mathrm{Ha}}\,h\right)\right\}, \end{aligned} \quad (12)$$

$$C(h) = \frac{Sh}{\mathrm{Ha}} - \frac{S}{\mathrm{Ha}^{3/2}}\tanh\left(\sqrt{\mathrm{Ha}}\,h\right). \quad (13)$$

It should be remarked that, when $\tau = 0$, the above terms agree with the long-wave equation derived by Tsai et al. [28] when the phase-change effects on the interface are neglected. The dimensionless parameters differ from the nondimensional set presented in Tsai et al. [28] because viscous scales are employed here. Although one can consider different scales, in principle, the structure of the evolution equation remains unchanged regardless of the dimensionless parameters appearing in the problem. Furthermore, the error in the second term associated with $B(h)$ in Tsai et al. [28] is corrected here, which as per the convention followed in their paper should read as $(4\alpha\,\mathrm{Re}\,h/m^5)\mathrm{sech}^2 mh\tanh mh$. Also, the case corresponding to $\mathrm{Ha} = 0$ can be recovered from (11)–(13) when $\mathrm{Ha} \to 0$. In this case, the functions in (11)–(13) read as

$$\begin{aligned} A(h) &= \mathrm{Re}\,h^2 + \tau h, \\ B(h) &= \frac{2}{15}\,\mathrm{Re}\,h^5\,(\mathrm{Re}\,h + \tau) - \frac{1}{3}\,\mathrm{Re}\,\cot\beta h^3, \\ C(h) &= S\frac{h^3}{3}, \end{aligned} \quad (14)$$

which match with the evolution equation derived by Miladinova et al. [9] in the absence of Marangoni and air shearing effect. The effect of magnetic field and air shear affects the leading order solution through $A(h)$ term in (11). This term contributes towards wave propagation and steepening mechanism. The effect of hydrostatic pressure is measured by the terms within the first flower bracket in $B(h)$ in (12). The rest of the terms in $B(h)$ affect the mean flow due to inertial, air shear and magnetic field contributions. The function $C(h)$ corresponds to the mean surface-tension effect. Although the effect of τ cannot be properly judged based on its appearance in (11)–(13), it is obvious that in the absence of the magnetic field both $A(h)$ and $B(h)$ increase (decrease) when $\tau > 0$ (< 0). The stability of the long-wave model (10) subject to (11)–(13) is investigated next.

4. Stability Analysis

The Nusselt solution corresponding to the problem is

$$h_0 = 1, \tag{15a}$$

$$u_0 = \frac{\sinh\left(\sqrt{\mathrm{Ha}}\, y\right)}{\sqrt{\mathrm{Ha}}}\left(\frac{\mathrm{Re}}{\sqrt{\mathrm{Ha}}}\tanh\sqrt{\mathrm{Ha}} + \tau\ \mathrm{sech}\sqrt{\mathrm{Ha}}\right) + \frac{\mathrm{Re}}{\mathrm{Ha}}\left(1 - \cosh\left(\sqrt{\mathrm{Ha}}\, y\right)\right), \tag{15b}$$

$$v_0 = 0, \tag{15c}$$

$$p_0 = \mathrm{Re}\,\cot\beta\,(1 - y). \tag{15d}$$

For a parallel shear flow, (10) subject to (11)–(13) admits normal mode solutions of the form $h = 1 + H(x,t)$, where $H(x,t)$ is the unsteady part of the film thickness representing the disturbance component such that $H \ll 1$ [56, 57]. Inserting $h = 1 + H(x,t)$ in (10) and invoking a Taylor series expansion about $h = 1$, the unsteady nonlinear equation representing a slight perturbation to the free surface is obtained as

$$\begin{aligned} &H_t + A_1 H_x + \varepsilon B_1 H_{xx} + \varepsilon C_1 H_{xxxx} \\ &\quad = -\left[A_1' H + \frac{A_1''}{2}H^2 + \frac{A_1'''}{6}H^3\right]H_x \\ &\qquad - \varepsilon\left[B_1' H + \frac{B_1''}{2}H^2\right]H_{xx} \\ &\qquad - \varepsilon\left(C_1' H + \frac{C_1''}{2}H^2\right)H_{xxxx} \\ &\qquad - \varepsilon\left[B_1' + B_1'' H\right](H_x)^2 \\ &\qquad - \varepsilon\left(C_1' + C_1'' H\right)H_x H_{xxx} + \mathcal{O}\left(\varepsilon H^4, H^5, \varepsilon^2 H\right), \end{aligned} \tag{16}$$

where (a prime denotes the order of the derivative with respect to h)

$$\begin{aligned} A_1 &= A(h=1), \qquad A_1' = A'(h=1), \\ A_1'' &= A''(h=1), \\ B_1 &= B(h=1), \qquad B_1' = B'(h=1), \\ B_1'' &= B''(h=1), \\ C_1 &= C(h=1), \qquad C_1' = C'(h=1), \\ C_1'' &= C''(h=1). \end{aligned} \tag{17}$$

It should be remarked that, while expanding the Taylor series, there are two small parameters, namely, $\varepsilon \ll 1$ and $H \ll 1$ whose orders of magnitude should be considered such that $\varepsilon \ll H \ll 1$. When $\mathcal{O}(\varepsilon H^3)$ terms are retained and since $\varepsilon H^3 \ll H^4$, $(A_1'''/6)H^3 H_x$ appears as a unique contribution of order H^4 in (16). This term, although present in the unsteady equation (16), does not contribute when a multiple-scale analysis is done (refer to Section 4.2.1 and Appendix B), where equations only up to $\mathcal{O}(\alpha^3)$ are considered while deriving a complex Ginzburg-Landau-type equation [12, 14, 17, 56, 57]. In addition, such a term did not appear in earlier studies [12, 14, 17, 56, 57] because $A(h)$ was a mathematical function of second degree in h, whose higher-order derivatives are zero.

Equation (16) forms the starting point for the linear stability analysis and describes the behavior of finite-amplitude disturbances of the film. Such an equation predicts the evolution of timewise behavior of an initially sinusoidal disturbance given to the film. It is important to note that the constant film thickness approximation with long-wave perturbations is a reasonable approximation only for certain segments of flow and implies that (16) is only locally valid.

4.1. Linear Stability. To assess the linear stability, the linear terms in (16) are considered. The unsteady part of the film thickness is decomposed as (a tilde denotes the complex conjugate)

$$H(x,t) = \eta e^{i(kx - C_L t) + C_R t} + \tilde{\eta} e^{-i(kx - C_L t) - C_R t}, \tag{18}$$

where η ($\ll 1$) is a complex disturbance amplitude independent of x and t. The complex eigenvalue is given by $\lambda = C_L + iC_R$ such that $k \in [0,1]$ represents the streamwise wavenumber. The linear wave velocity and the linear growth rate (amplification rate) of the disturbance are C_L/k, $C_R \in (-\infty, \infty)$, respectively. Explicitly, they are found as

$$\begin{aligned} C_{LV} &= \frac{C_L}{k} = A_1, \\ C_R &= \varepsilon k^2\left(B_1 - k^2 C_1\right). \end{aligned} \tag{19}$$

The disturbances grow (decay) when $C_R > 0$ ($C_R < 0$). However, when $C_R = 0$, the curve $k = 0$ and the positive branch of $k^2 = B_1/C_1$ represent the neutral stability curves. Identifying the positive branch of $B_1 - k^2 C_1 = 0$ as $k_c = \sqrt{(B_1/C_1)}$ (k_c is the critical wavenumber), the wavenumber k_m corresponding to the maximal growth rate is obtained from $(\partial/\partial k)C_R = 0$. This gives $B_1 - 2k_m^2 C_1 = 0$ such that $k_m = k_c/\sqrt{2}$. The linear amplification of the most unstable mode is calculated from $C_R|_{k=k_m}$.

A parametric study considering the elements of the set $\mathbb{S} = \{\mathrm{Re}, \mathrm{Ha}, S, \beta, \tau\}$ is done in order to trace the neutral stability and linear amplification curves by assuming the slenderness parameter to be 0.1. Only those curves which are relevant in drawing an opinion are presented.

The influence of the magnetic field on the critical Reynolds number (Re_c) varying as a function of the shear parameter is presented in Figure 2. For each Ha, there is a Re_c below which the flow is stable. The critical Reynolds number decreases when the angle of inclination increases, and, therefore, the flow destabilizes. The stabilizing effect of the magnetic field is also seen when Ha increases. There exists a certain $\tau > 0$ such that the flow remains unstable beyond it.

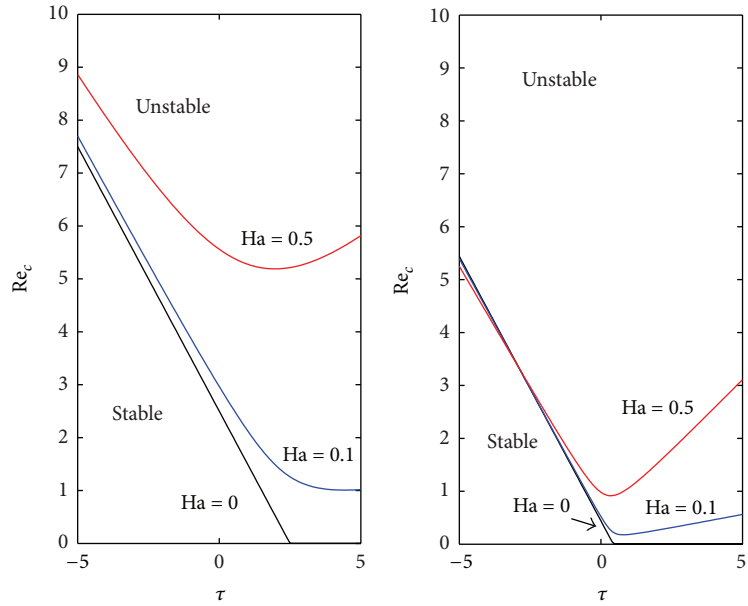

FIGURE 2: Critical Reynolds number as a function of τ when $S = 0$: (a) $\beta = 45^\circ$; (b) $\beta = 80^\circ$.

Figures 3 and 4 display the neutral stability curves, which divide the $k - \mathrm{Re}$ and $k - \tau$ planes into regions of stable and unstable domains. On the other hand, Figure 5 shows the linear amplification curves. The shear stress offered by the air destabilizes the flow when it flows along the downhill direction ($\tau > 0$) and increases the instability threshold compared to the case corresponding to $\tau = 0$ (Figures 3 and 4). However, the flow mechanism is better stabilized when the applied shear stress offered by the air is in the uphill direction ($\tau < 0$) than when $\tau = 0$ (Figures 3 and 4). As seen from Figure 3, the portion of the axis corresponding to the unstable Reynolds numbers increases and extends towards the left when the angle of inclination increases, thereby reducing the stabilizing effect offered by the hydrostatic pressure at small inclination angles. From curves 2 and 3 corresponding to Figure 3, it is observed that the force of surface-tension stabilizes the flow mechanism. Figure 4 supports the information available from Figure 3. When the magnitude of the Hartmann number increases, the instability region decreases because the value of the critical wavenumber decreases. Comparing Figure 4(a) with Figure 4(c), it is also observed that the inertial force destabilizes the flow mechanism. The growth rate curves (Figure 5) agree with the results offered by the neutral stability curves (Figures 3 and 4).

The linearly increasing graphs of C_L and the decreasing plots of C_{LV} with respect to k and Ha, respectively, are presented in Figure 6. The effect of inertia doubles the linear wave speed, C_{LV}. But when the magnitude of Ha, increases, the linear wave speed decreases. The downhill effect of the shear stress on the interface makes the linear wave speed larger than the cases corresponding to $\tau = 0$ and $\tau < 0$.

The linear stability results give only a firsthand information about the stability mechanism. The influence of air-induced shear on the stability of the flow under the application of a transverse magnetic field will be better understood only when the nonlinear effects are additionally considered. To analyze and illustrate the nonlinear effects on the stability threshold, a weakly nonlinear study is performed in the next step.

4.2. Multiple-Scale Analysis

4.2.1. Weakly Nonlinear Theory. In order to do multiple-scale analysis, the following slow scales are introduced following Sadiq and Usha [14] (the justification for stretching the scales is provided in Lin [56] and in Krishna and Lin [57]):

$$t_1 = \alpha t, \qquad t_2 = \alpha^2 t, \qquad x_1 = \alpha x, \tag{20}$$

such that

$$\frac{\partial}{\partial t} \longrightarrow \frac{\partial}{\partial t} + \alpha \frac{\partial}{\partial t_1} + \alpha^2 \frac{\partial}{\partial t_2},$$
$$\frac{\partial}{\partial x} \longrightarrow \frac{\partial}{\partial x} + \alpha \frac{\partial}{\partial x_1}. \tag{21}$$

Here, α is a small parameter independent of ε and measures the distance from criticality such that $C_R \sim \mathcal{O}(\alpha^2)$ (or, $B_1 - k^2 C_1 \sim \mathcal{O}(\alpha^2)$). The motivation behind such a study lies in deriving the complex Ginzburg-Landau equation (CGLE), which describes the evolution of amplitudes of unstable modes for any process exhibiting a Hopf bifurcation. Using such an analysis, it is possible to examine whether the

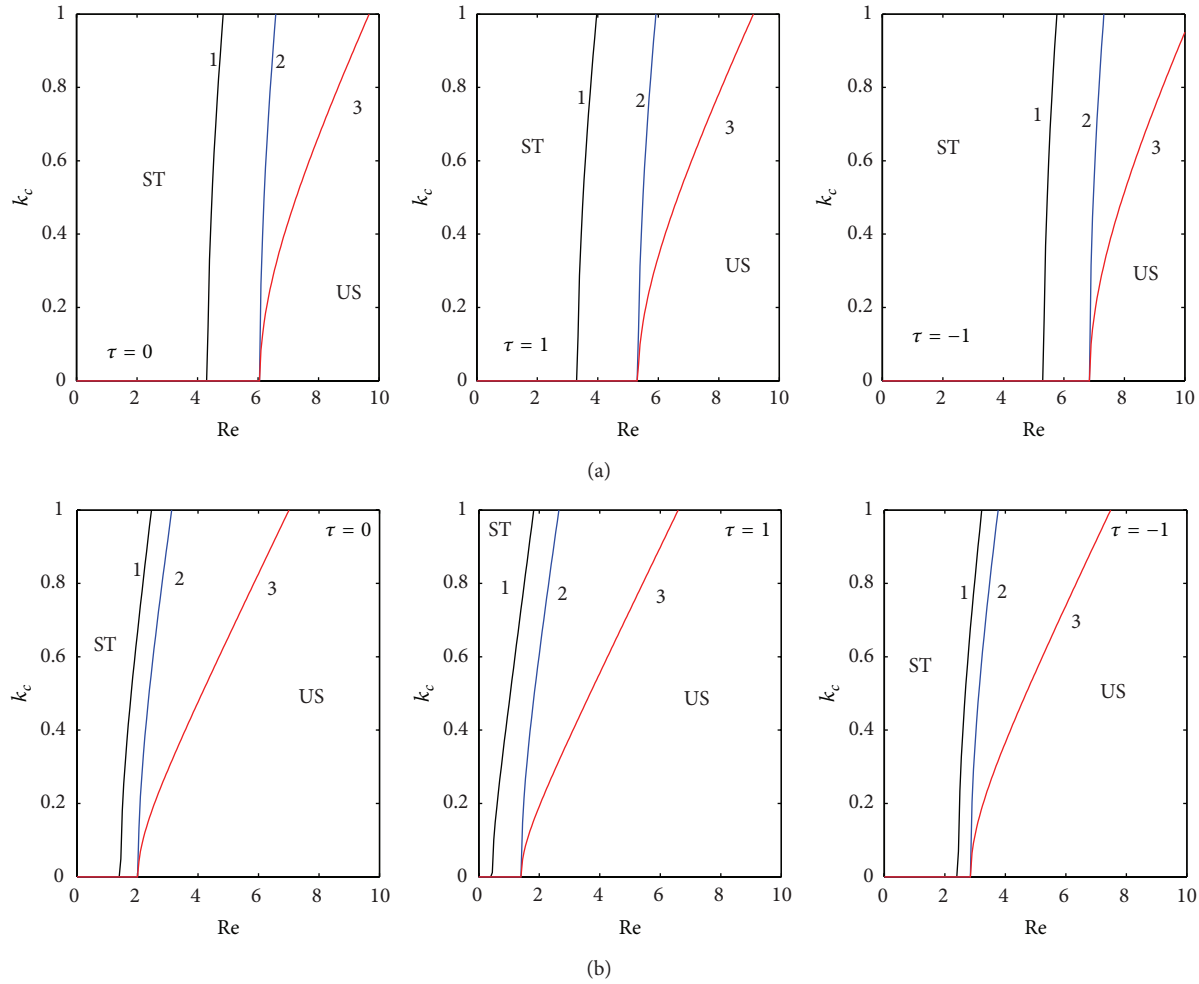

Figure 3: Neutral stability curves. The symbols ST and US indicate the stable and unstable regions. Here, (1) Ha = 0.001 and $S = 1$; (2) Ha = 0.2 and $S = 1$; (3) Ha = 0.2 and $S = 10$. (a) $\beta = 30^\circ$ and (b) $\beta = 60^\circ$.

nonlinear waves in the vicinity of criticality attain a finite height and remain stable or continue to grow in time and eventually become unstable. Refer to Appendix B for the detailed derivations of the threshold amplitude, $\alpha\Gamma_0$, and the nonlinear wave speed, N_c.

The threshold amplitude subdivides the flow domain according to the signs of C_R and J_2 [14]. If $C_R < 0$ and $J_2 < 0$, the flow exhibits subcritical instability. However, when $C_R > 0$ and $J_2 > 0$, the Landau state is supercritically stable. If, on the other hand, $C_R < 0$ and $J_2 > 0$, the flow is subcritically stable. A blow-up supercritical explosive state is observed when $C_R > 0$ and $J_2 < 0$.

Different regions of the instability threshold obtained through multiple-scale analysis are illustrated in Figure 7. The subcritical unstable region is affected due to the variation of τ. For $\tau < 0$, such a region is larger than the ones corresponding to $\tau \geq 0$. In addition, the subcritical unstable and the stable regions increase when Ha increases. The explosive state region (also called the nonsaturation zone) decreases when $\tau < 0$ than when $\tau \geq 0$. The strip enclosing asterisks is the supercritical stable region where the flow, although linearly unstable, exhibits a finite-amplitude behavior and saturates as time progresses [8, 9, 14]. The bottom line of the strip is the curve $k_s = k_c/2$ which separates the supercritical stable region from the explosive region [56, 58, 59]. Within the strip $k_s < k < k_c$, different possible shapes of the waves exist [7, 9, 14].

Tables 1 and 2 show the explosive and equilibration state values for different flow parameters. The wavenumber value corresponding to the explosive state increases when the inertial effects increase. This increases the unstable region $0 < k < k_s$ (Table 1). Such a wavenumber decreases either when the hydromagnetic effect is increased or when the air shear is in the uphill direction. It is evident from Table 1 that the explosive state occurs at small values of Re and β, which is also true for large values of Ha when $\tau < 0$. Also, it is observed that either when the Hartmann number or the value of the uphill shear is increased, the critical wavenumber becomes zero (Table 2). Therefore, $k_s = 0$ (Table 1).

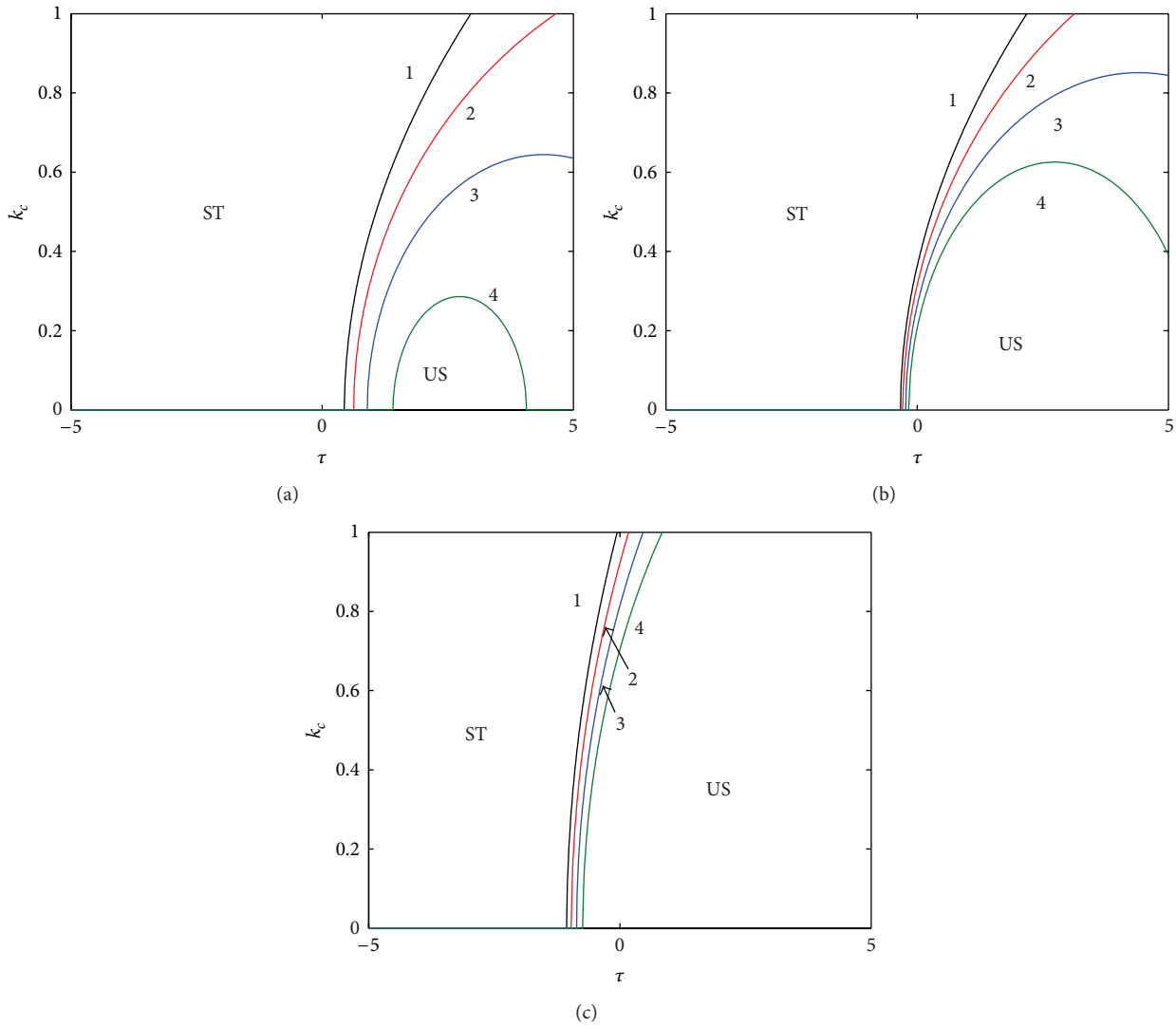

FIGURE 4: Neutral stability curves in the $k - \tau$ plane for $S = 1$: (1) Ha = 0; (2) Ha = 0.05; (3) Ha = 0.1; and (4) Ha = 0.15. (a) $\beta = 60^\circ$ and Re = 1; (b) $\beta = 75^\circ$ and Re = 1; and (c) $\beta = 60^\circ$ and Re = 2.5.

The threshold amplitude ($\alpha\Gamma_0$) profiles display an asymmetric structure (Figure 8), increasing up to a certain wavenumber ($>k_m$) and then decreasing beyond it in the supercritical stable region. The $\tau > 0$ induced amplitudes show larger peak amplitude than the cases corresponding to $\tau = 0$ and $\tau < 0$. The peak amplitude value decreases when Ha increases. The nonlinear wave speed (N_c) curves represent a 90° counterclockwise rotation of the mirror image of the alphabet L when Ha is small. The nonlinear speed decreases to a particular value in the vertical direction and thereafter traces a constant value beyond it as the wavenumber increases in the supercritical stable region. However, when the effect of the magnetic field is increased, the nonlinear wave speed decreases in magnitude and sketches an almost linear constant profile. The magnitude of N_c in the supercritical stable region corresponding to $\tau = 0$ remains inbetween the values corresponding to $\tau < 0$ and $\tau > 0$.

4.2.2. Sideband Instability. Let us consider the quasi-monochromatic wave of (B.4) exhibiting no spatial modulation of the form

$$\eta = \Gamma_s(t_2) = \Gamma_0 e^{-ibt_2}, \tag{22}$$

where Γ_0 and b are defined by (B.10) and (B.11) such that $\omega_s + b$ is the wave frequency and $k(> 0)$ is the modulation wavenumber.

If one considers a band of frequencies centered around ω_s, the interaction of one side-mode with the second harmonic would be resonant with the other side-mode causing the frequency to amplify. This leads to an instability known as sideband instability [60, 61].

To investigate such an instability, $\Gamma_s(t_2)$ is subjugated to sideband disturbances of bandwidth $k\alpha$ [12, 56, 57].

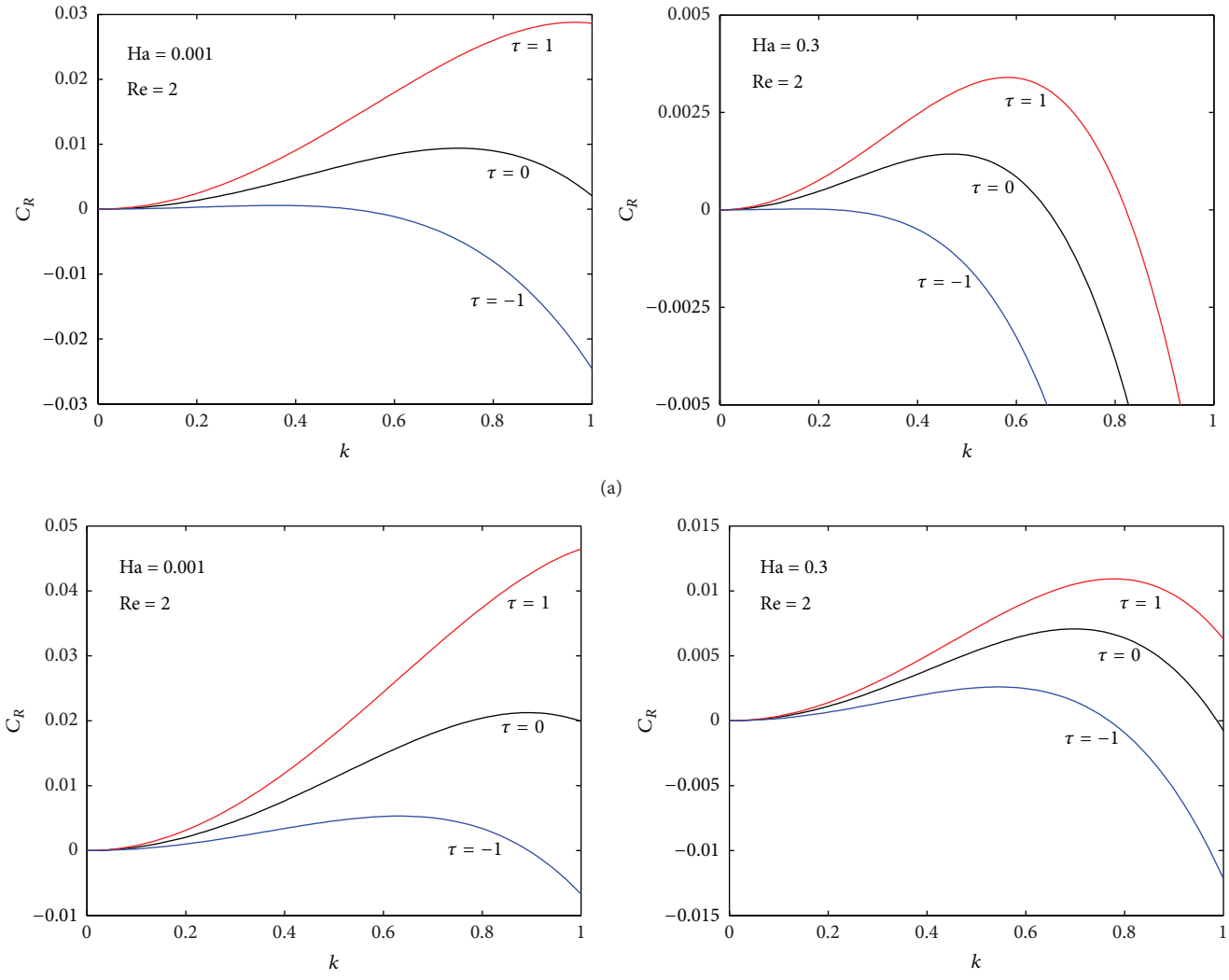

FIGURE 5: Growth rate curves when We = 1: (a) $\beta = 75^\circ$ and (b) $\beta = 90^\circ$.

The explicit expression for the eigenvalues is found as (refer to Appendix C)

$$\begin{aligned}\vartheta &= \frac{1}{2}\left(\operatorname{tr}(\mathscr{M}) \pm \sqrt{\operatorname{tr}^2(\mathscr{M}) - 4\det(\mathscr{M})}\right)\\ &= -c_i + k^2 J_{1r} \pm \frac{1}{2}\sqrt{4\left(c_i^2 + k^2\nu^2\right) - \frac{8iJ_4 c_i \nu k}{J_2}}\\ &= \varpi_1 \pm \varpi_2,\end{aligned} \tag{23}$$

where

$$\begin{aligned}\operatorname{tr}(\mathscr{M}) &= 2c_i + 2k^2 J_{1r} - 4J_2\left|\Gamma_s\right|^2 = -2c_i + 2k^2 J_{1r},\\ \det(\mathscr{M}) &= J_1^2 k^4 - \left(\nu^2 + 2c_i J_1\right)k^2 - \frac{2ic_i \nu J_4}{J_2}k.\end{aligned} \tag{24}$$

It should be remarked that the above expression for ϑ is true only if $\nu \sim \mathcal{O}(\alpha)$. However, when $\nu = 0$, it is easily seen from (23) that $\vartheta_1 = \varpi_1 + \varpi_2 = k^2 J_{1r} < 0$ and $\vartheta_2 = \varpi_1 - \varpi_2 = -2c_i + k^2 J_{1r} < 0$ (when $c_i > 0$), implying that the system is stable to the sideband disturbances as $t_2 \to \infty$. For nonzero ν, the eigenvalues depend on the dimensionless flow parameters. If $\varpi_2 > 0$ and is less than the absolute value of ϖ_1, the sideband modes stabilize the system as $t_2 \to \infty$. However, if $\varpi_2 > 0$ and is greater than the absolute value of ϖ_1, only one of the modes is sideband stable. On the other hand, if $(c_i^2 + k^2\nu^2) - (8iJ_4 c_i \nu k \setminus J_2) < 0$, again, one of the modes is sideband stable.

5. Equilibria of a Bimodal Dynamical System

Considering the initial thickness of the amplitude to be one, Gjevik [58] analyzed the amplitude equations by representing the amplitude using a truncated Fourier series and by imposing restrictions on its coefficients. The velocity along the mean flow direction and the corresponding surface deflection moving with this velocity were deduced by posing

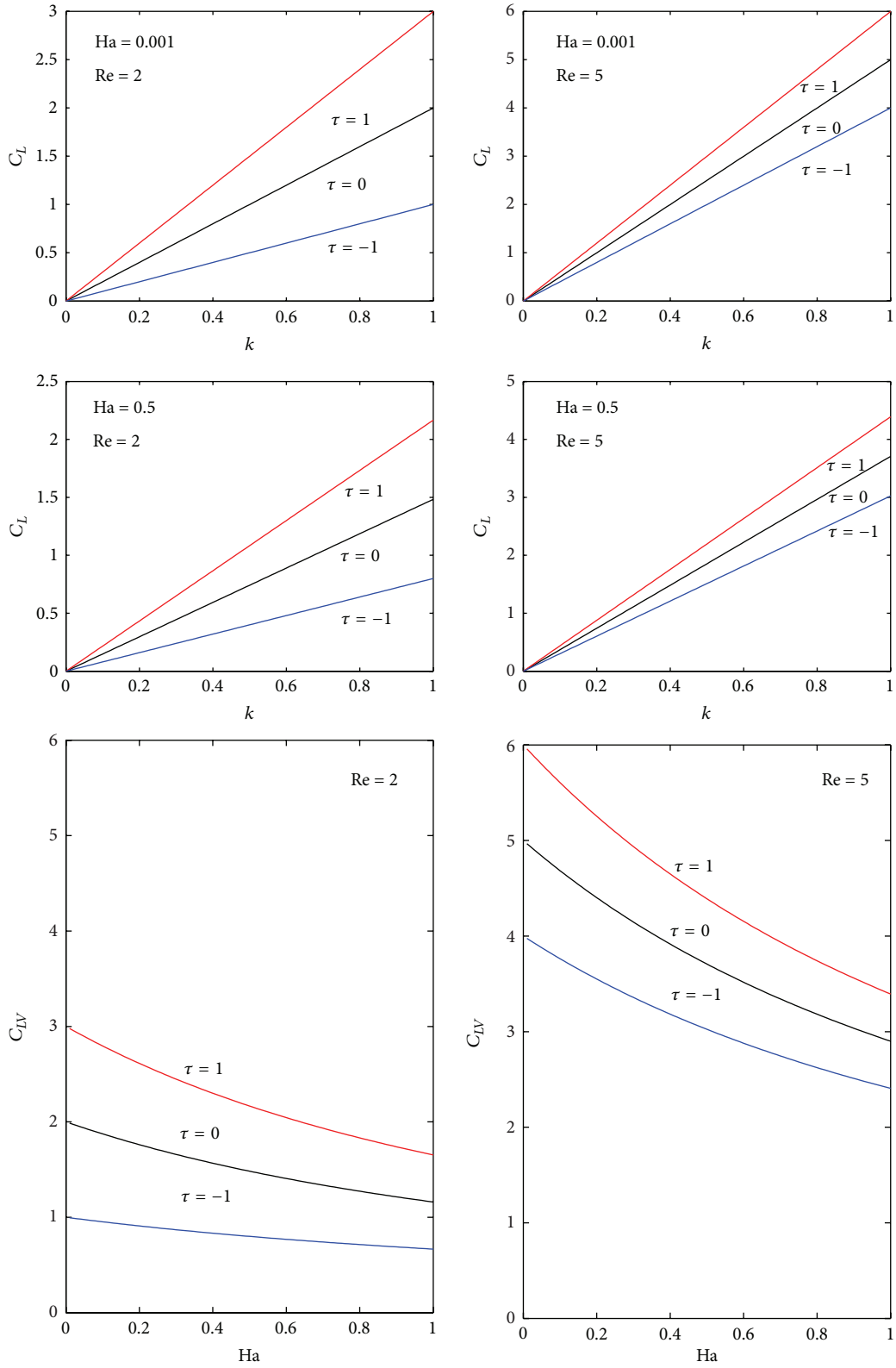

Figure 6: Variation of the linear wave velocity, C_{LV}, with respect to Ha, and C_L versus k.

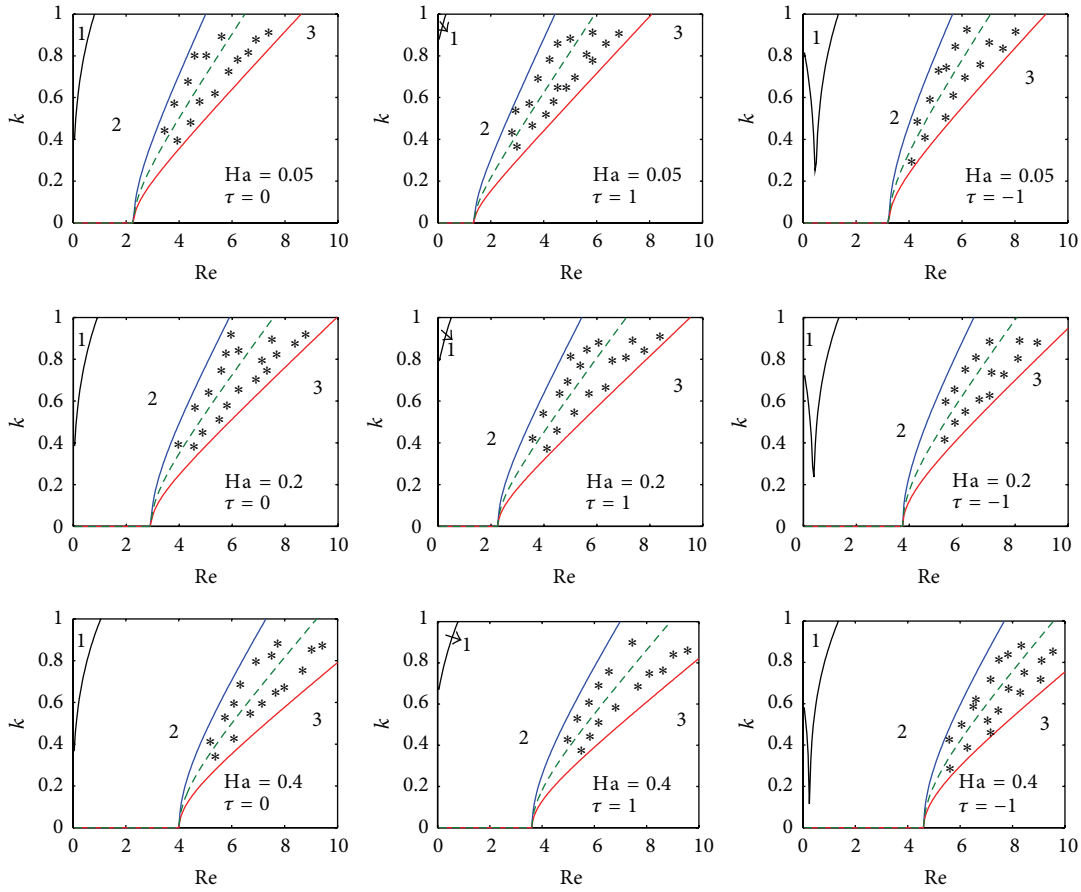

FIGURE 7: Variation of k with respect to Re when $\beta = 50^{\circ}$ and $S = 5$: (1) $C_R < 0$ and $J_2 < 0$; (2) $C_R < 0$ and $J_2 > 0$; (3) $C_R > 0$ and $J_2 < 0$. The strip enclosing asterisks indicates that $C_R > 0$ and $J_2 > 0$. The broken line within the strip represents $k_m = k_c/\sqrt{2}$.

the problem into a dynamical system. Gottlieb and Oron [62] and Dandapat and Samanta [12] also expanded the evolution equation using a truncated Fourier series to derive a modal dynamical system. The results in Gottlieb and Oron [62] showed that a two-mode model was found to coincide with the numerical solution along the Hopf bifurcation curve. Based on this confidence, the stability of the bimodal dynamical system was assessed in Dandapat and Samanta [12].

In this section, the stability of a truncated bimodal dynamical system is analyzed using the approach followed by the above authors, but using the assumptions considered in Gjevik [58]. The coupled dynamical system and its entries are listed in Appendix D.

It should be remarked that in the k − Re plane the equations $b_{111} = 0$ and $\partial[kb_{111}]/\partial k = 0$ give the neutral stability curve and the curve corresponding to the maximum rate of amplification for linear disturbances. The expression

$$v_c = \frac{d}{dt}\theta_1(t) = c_{111} + \left[c_{121}\cos\phi(t) - b_{121}\sin\phi(t)\right] \times a_2(t) + c_{131}a_1^2(t) + c_{132}a_2^2(t) \quad (25)$$

measures the velocity along the direction of the mean flow of a steady finite-amplitude wave. The surface deflection, $h(x,t)$, moving with velocity v_c along the mean flow direction in a coordinate system $x' = x + \theta_1$ is calculated from (D.1) and reads as

$$h(x,t) = 1 + 2\left[B_1\cos x' + B_2\cos\left(2x' - \phi\right)\right]. \quad (26)$$

The steady solutions of the system (D.2a) and (D.2b) correspond to the fixed points of (D.4a)–(D.4c). In addition to the trivial solution $a_1(t) = 0$, $a_2(t) = 0$, and $\phi(t) = 0$ ($z_1(t) = 0; z_2(t) = 0$), system (D.4a)–(D.4c) offers nontrivial fixed points [62–64]. These fixed points can be classified as pure-mode fixed points (where one of the fixed points is zero and the others are nonzero), mixed-mode fixed points (nonzero fixed points with a zero or nonzero phase difference), and traveling waves with nonzero constant phase difference.

5.1. Pure-Mode. The fixed points in this case are obtained by setting $f_i(a_1, a_2, \phi) = 0$, $i = 1, 2, 3$, in (D.4a)–(D.4c). This gives $a_1(t) = 0$ and $a_2^2(t) = -b_{211}/b_{232}$. The solution exists if $\mathrm{sgn}(b_{211}b_{232}) = -1$. For convenience, $a_2^2(t) = \tilde{a}^2$ is set. From

Table 1: Parameter values for which the nonlinear wave explodes.

		$\beta = 55^\circ$		$\beta = 75^\circ$	
		Re = 3	Re = 6	Re = 3	Re = 6
$\tau = 1$	Ha = 0	$k_s = 0.3671$	$k_s = 0.7933$	$k_s = 0.4467$	$k_s = 0.8707$
	Ha = 0.2	$k_s = 0.2309$	$k_s = 0.6056$	$k_s = 0.3438$	$k_s = 0.7045$
	Ha = 0.4	$k_s = 0.0268$	$k_s = 0.4399$	$k_s = 0.2561$	$k_s = 0.5686$
$\tau = 0$	Ha = 0	$k_s = 0.2733$	$k_s = 0.7132$	$k_s = 0.3734$	$k_s = 0.7992$
	Ha = 0.2	$k_s = 0.1536$	$k_s = 0.5517$	$k_s = 0.2974$	$k_s = 0.6588$
	Ha = 0.4	$k_s = 0$	$k_s = 0.4073$	$k_s = 0.2319$	$k_s = 0.5436$
$\tau = -1$	Ha = 0	$k_s = 0.1211$	$k_s = 0.6237$	$k_s = 0.2823$	$k_s = 0.7205$
	Ha = 0.2	$k_s = 0$	$k_s = 0.4861$	$k_s = 0.2301$	$k_s = 0.6049$
	Ha = 0.4	$k_s = 0$	$k_s = 0.3602$	$k_s = 0.1835$	$k_s = 0.5094$

Table 2: Parameter values for which the nonlinear wave attains a finite amplitude.

		$\beta = 55^\circ$		$\beta = 75^\circ$	
		Re = 3	Re = 6	Re = 3	Re = 6
$\tau = 1$	Ha = 0	$k_c = 0.7342$	$k_c = 1.5866$	$k_c = 0.8933$	$k_c = 1.7415$
	Ha = 0.2	$k_c = 0.4618$	$k_c = 1.2112$	$k_c = 0.6875$	$k_c = 1.4092$
	Ha = 0.4	$k_c = 0.0536$	$k_c = 0.8799$	$k_c = 0.5121$	$k_c = 1.1371$
$\tau = 0$	Ha = 0	$k_c = 0.5467$	$k_c = 1.4263$	$k_c = 0.7468$	$k_c = 1.5984$
	Ha = 0.2	$k_c = 0.3071$	$k_c = 1.1034$	$k_c = 0.5947$	$k_c = 1.3177$
	Ha = 0.4	$k_c = 0$	$k_c = 0.8145$	$k_c = 0.4638$	$k_c = 1.0872$
$\tau = -1$	Ha = 0	$k_c = 0.2421$	$k_c = 1.2475$	$k_c = 0.5646$	$k_c = 1.4411$
	Ha = 0.2	$k_c = 0$	$k_c = 0.9722$	$k_c = 0.4602$	$k_c = 1.2099$
	Ha = 0.4	$k_c = 0$	$k_c = 0.7205$	$k_c = 0.1834$	$k_c = 1.0187$

(D.4c), $c_{121}\cos\phi(t) - b_{121}\sin\phi(t) = (k/2)A_1''a$ is obtained. From this condition, the fixed point for $\phi(t)$ is derived as

$$\phi(t) = \tilde{\phi}(t) = \tan^{-1}\left[\left(4b_{121}c_{121} \pm kA_1''\tilde{a} \times \left\{4b_{121}^2 + 4c_{121}^2 - k^2A_1''^2\tilde{a}^2\right\}^{1/2}\right) \times \left(4b_{121}^2 - k^2A_1''^2\tilde{a}^2\right)^{-1}\right], \tag{27}$$

provided that the quantity within the square root is real and positive. The stability of the nonlinear dynamical system (D.4a)–(D.4c) can be locally evaluated using the eigenvalues of the matrix obtained after linearizing the system around the fixed points. The linear approximation of the dynamical system (D.4a)–(D.4c) can be represented in matrix notation as

$$\begin{pmatrix} \frac{da_1(t)}{dt} \\ \frac{da_2(t)}{dt} \\ \frac{d\phi(t)}{dt} \end{pmatrix} = \begin{pmatrix} p_1 & 0 & 0 \\ 0 & p_2 & 0 \\ 0 & p_3 & p_4 \end{pmatrix} \begin{pmatrix} a_1(t) \\ a_2(t) \\ \phi(t) \end{pmatrix} + \begin{pmatrix} q_1 \\ q_2 \\ q_3 \end{pmatrix}, \tag{28}$$

such that

$$\begin{aligned} p_1 &= b_{111} + \left(b_{121}\cos\tilde{\phi} + c_{121}\sin\tilde{\phi}\right)\tilde{a} + b_{132}\tilde{a}^2; \\ p_2 &= b_{211} + 3b_{232}\tilde{a}^2, \\ p_3 &= -2b_{121}\sin\tilde{\phi} + 2c_{121}\cos\tilde{\phi} - 2kA_1''\tilde{a}; \\ p_4 &= -\left(2b_{121}\cos\tilde{\phi} + 2c_{121}\sin\tilde{\phi}\right)\tilde{a}, \\ q_1 &= 0; \qquad q_2 = -2b_{232}\tilde{a}^3; \\ q_3 &= kA_1''\tilde{a}^2 + \left(2b_{121}\cos\tilde{\phi} + 2c_{121}\sin\tilde{\phi}\right)\tilde{\phi}\tilde{a}. \end{aligned} \tag{29}$$

The stability of the linear system (28) depends on the eigenvalues of the coefficient matrix with entries p_i. The eigenvalues are found as

$$\begin{aligned} \lambda_1 &= b_{211} + 3\tilde{a}^2b_{232} = -2b_{211}, \\ \lambda_2 &= -2\tilde{a}\left(b_{121}\cos\tilde{\phi} + c_{121}\sin\tilde{\phi}\right), \\ \lambda_3 &= b_{111} + \tilde{a}\left(b_{121}\cos\tilde{\phi} + c_{121}\sin\tilde{\phi}\right) + b_{132}\tilde{a}^2. \end{aligned} \tag{30}$$

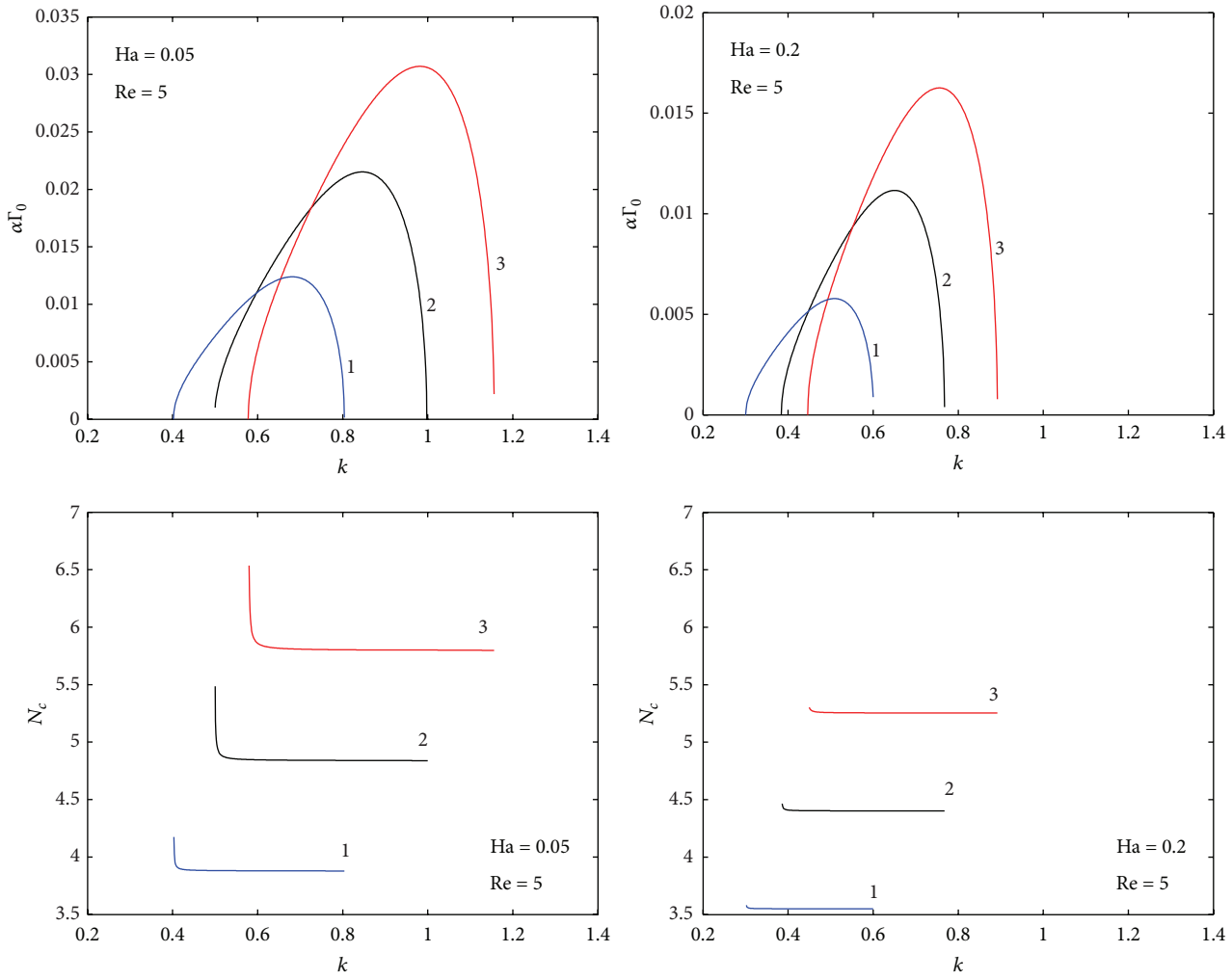

FIGURE 8: Threshold amplitude and nonlinear wave speed in the supercritical stable region for $\beta = 50^\circ$ and $S = 5$: (1) $\tau = -1$, (2) $\tau = 0$, and (3) $\tau = 1$.

The Hopf bifurcation at the critical threshold is defined by $B_1 = k^2 C_1$, and this yields $\lambda_1 = 24\varepsilon k^4 C_1 > 0$. This eigenvalue being independent of τ increases when the effects of surface-tension and Hartmann number increase. Therefore, at the critical threshold, the fixed points corresponding to the pure-mode are unstable. Beyond the neutral stability limit where the flow is linearly stable ($C_R < 0$) and where the stable wavenumber region decreases when the direction of the shear offered by the wind changes from uphill to downhill direction, the eigenvalue may remain positive and still destabilize the system as shown in Figure 9. The stable wavenumbers corresponding to the linear stability threshold (refer to Figure 5 with Ha = 0.3 and Re = 2) are considered to plot the eigenvalue λ_1. Although the magnitude of λ_1 remains larger for $\tau < 0$ than for $\tau \geq 0$, being positive, it plays a destabilizing role.

5.2. Mixed-Mode. When $a_1(t), a_2(t) \neq 0$, the fixed points in this case correspond to mixed-mode. Considering $\phi(t) \neq 0$ and a_1^*, a_2^*, and ϕ^* to be the fixed points of (D.4a)–(D.4c), the nonlinear system can be linearized around the fixed points. Then, the stability (instability) of the fixed points demands all of the eigenvalues of the linearized Jacobian matrix to be negative (at least one of them to be positive). The nine entries t_{ij} $(i, j = 1, 2, 3)$ of the 3×3 Jacobian matrix arising due to linearization are the following:

$$t_{11} = b_{111} + \left(b_{121}\cos\phi^* + c_{121}\sin\phi^*\right)a_2^* + 3b_{131}a_1^{*2} + b_{132}a_2^{*2},$$

$$t_{12} = \left(b_{121}\cos\phi^* + c_{121}\sin\phi^*\right)a_1^* + 2b_{132}a_1^*a_2^*,$$

$$t_{13} = \left(-b_{121}\sin\phi^* + c_{121}\cos\phi^*\right)a_1^*a_2^*,$$

$$t_{21} = 2\left(b_{221}\cos\phi^* - c_{221}\sin\phi^*\right)a_1^* + 2b_{231}a_1^*a_2^*,$$

$$t_{22} = b_{211} + b_{231}a_1^{*2} + 3b_{232}a_2^{*2},$$

$$t_{23} = -\left(b_{221}\sin\phi^* + c_{221}\cos\phi^*\right)a_1^{*2},$$

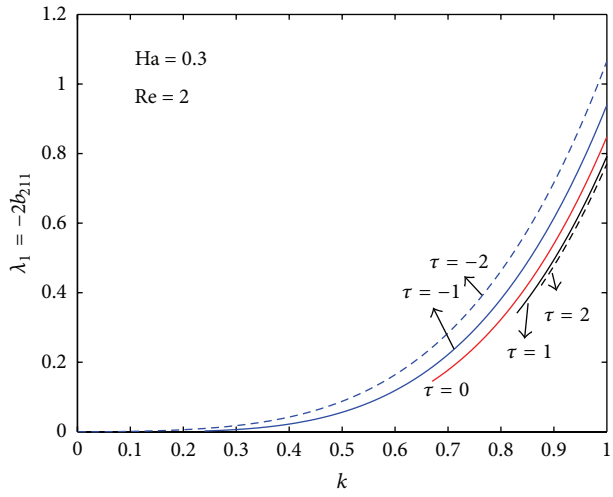

FIGURE 9: Eigenvalue λ_1 as a function of k when We = 1 and $\beta = 75^\circ$.

$$
\begin{aligned}
t_{31} &= 2kA_1''a_1^* - \frac{2a_1^*}{a_2^*}\left(b_{221}\sin\phi^* + c_{221}\cos\phi^*\right),\\
t_{32} &= -2kA_1''a_2^* + 2\left(c_{121}\cos\phi^* - b_{121}\sin\phi^*\right)\\
&\quad + \frac{a_1^{*2}}{a_2^{*2}}\left(b_{221}\sin\phi^* + c_{221}\cos\phi^*\right),\\
t_{33} &= -2\left(c_{121}\sin\phi^* + b_{121}\cos\phi^*\right)a_2^*\\
&\quad - \left(b_{221}\cos\phi^* - c_{221}\sin\phi^*\right)\frac{a_1^{*2}}{a_2^*}.
\end{aligned}
\tag{31}
$$

It should be remarked that Samanta [65] also discussed the mixed-mode for the flow of a thin film on a nonuniformly heated vertical wall. However, it should be noted that the Jacobian was computed not by considering a zero phase difference with $a_1(t), a_2(t) \neq 0$, but by evaluating the Jacobian first by imposing $a_1(t), a_2(t), \phi(t) \neq 0$ and then by substituting $\phi = 0$ in the computed Jacobian. If one considers $a_1(t), a_2(t), \phi(t) = 0$, an overdetermined system is obtained.

5.3. Traveling Waves. Fixed points of (D.4a)–(D.4c) with ϕ being a nonzero constant correspond to traveling waves. The modal amplitudes are considered small in the neighborhood of the neutral stability limit. After rescaling $a_1(t) \to \alpha m_1(t)$ and $a_2(t) \to \alpha^2 m_2(t)$, the following system is obtained:

$$
\begin{aligned}
\frac{dm_1(t)}{dt} &= b_{111}m_1(t) + \alpha^2\\
&\quad \times \left[b_{121}\cos\phi(t) + c_{121}\sin\phi(t)\right]m_1(t)\,m_2(t)\\
&\quad + \alpha^2 b_{131}m_1^3(t) + \mathcal{O}\left(\alpha^4\right),
\end{aligned}
\tag{32a}
$$

$$
\begin{aligned}
\frac{dm_2(t)}{dt} &= b_{211}m_2(t)\\
&\quad + \left[b_{221}\cos\phi(t) - c_{221}\sin\phi(t)\right]m_1^2(t)\\
&\quad + \alpha^2 b_{231}m_1^2(t)\,m_2(t) + \mathcal{O}\left(\alpha^4\right),
\end{aligned}
\tag{32b}
$$

$$
\begin{aligned}
\frac{d\phi(t)}{dt} &= -\left[b_{221}\sin\phi(t) + c_{221}\cos\phi(t)\right]\frac{m_1^2(t)}{m_2(t)}\\
&\quad + \alpha^2 kA_1''m_1^2(t) + 2\alpha^2\\
&\quad \times \left[c_{121}\cos\phi(t) - b_{121}\sin\phi(t)\right]m_2(t) + \mathcal{O}\left(\alpha^4\right).
\end{aligned}
\tag{32c}
$$

To the $\mathcal{O}(\alpha^2)$, there are no nontrivial fixed points in the above system. The phase evolution is governed by equating the right-hand side of (32c) to zero by considering terms up to $\mathcal{O}(\alpha^2)$:

$$
\tan\phi(t) = \frac{\left(-l_1l_2 \pm l_3\left(l_1^2 + l_2^2 - l_3^2\right)^{1/2}\right)}{\left(l_1^2 - l_3^2\right)},
\tag{33}
$$

where $l_1 = (1 + 2\alpha^2 b_{121}m_2^2(t)/b_{221}m_1^2(t))$, $l_2 = (c_{221}/b_{221}) - (2\alpha^2 c_{121}m_2^2(t)/b_{221}m_1^2(t))$, and $l_3 = \alpha^2 kA_1''m_2(t)/b_{221}$. In the above equation, if only the leading order effect is considered, the fixed point is found as

$$
\phi^*(t) = \tan^{-1}\left(\frac{-c_{221}}{b_{221}}\right) + \mathcal{O}\left(\alpha^2\right).
\tag{34}
$$

Equating (32a) to zero and using (34), it is found that

$$
\alpha^2 b_{131}m_1^2(t) = -b_{111} - \alpha^2\varphi_1 m_2(t).
\tag{35}
$$

Such a solution exists if $[b_{111} + \alpha^2\varphi_1 m_2(t)]b_{131} < 0$, where $\varphi_1 = (b_{121}\cos\phi^* + c_{121}\sin\phi^*)$. A quadratic equation in $m_2(t)$ is obtained by considering (32b) as

$$
\begin{aligned}
&\alpha^4 b_{231}\varphi_1 m_2^2(t) + \alpha^2\left(b_{111}b_{231} - b_{211}b_{131} + \varphi_1\varphi_2\right)\\
&\quad \times m_2(t) + \varphi_2 b_{111} = 0,
\end{aligned}
\tag{36}
$$

where $\varphi_2 = b_{221}\cos\phi^* - c_{221}\sin\phi^*$. For this equation, there are two solutions. The existence of such solutions to be a real number demands $(b_{111}b_{231} - b_{211}b_{131} + \varphi_1\varphi_2)^2 - 4\alpha^4\varphi_1\varphi_2 b_{111}b_{231} > 0$. Since $b_{111} = 0$ in the neutral stability limit, (36) gives the amplitude of the nonzero traveling wave as

$$
m_2(t) = \frac{b_{211}b_{131} - \varphi_1\varphi_2}{\alpha^2 b_{231}\varphi_1} = \frac{3k^2C_1J_2}{\alpha^2\left(B_1'' - 4k^2C_1''\right)\varphi_1}.
\tag{37}
$$

When $J_2 = 0$, $m_2(t)$ is zero, and this corresponds to finding the critical Reynolds number in the neutral stability limit [12].

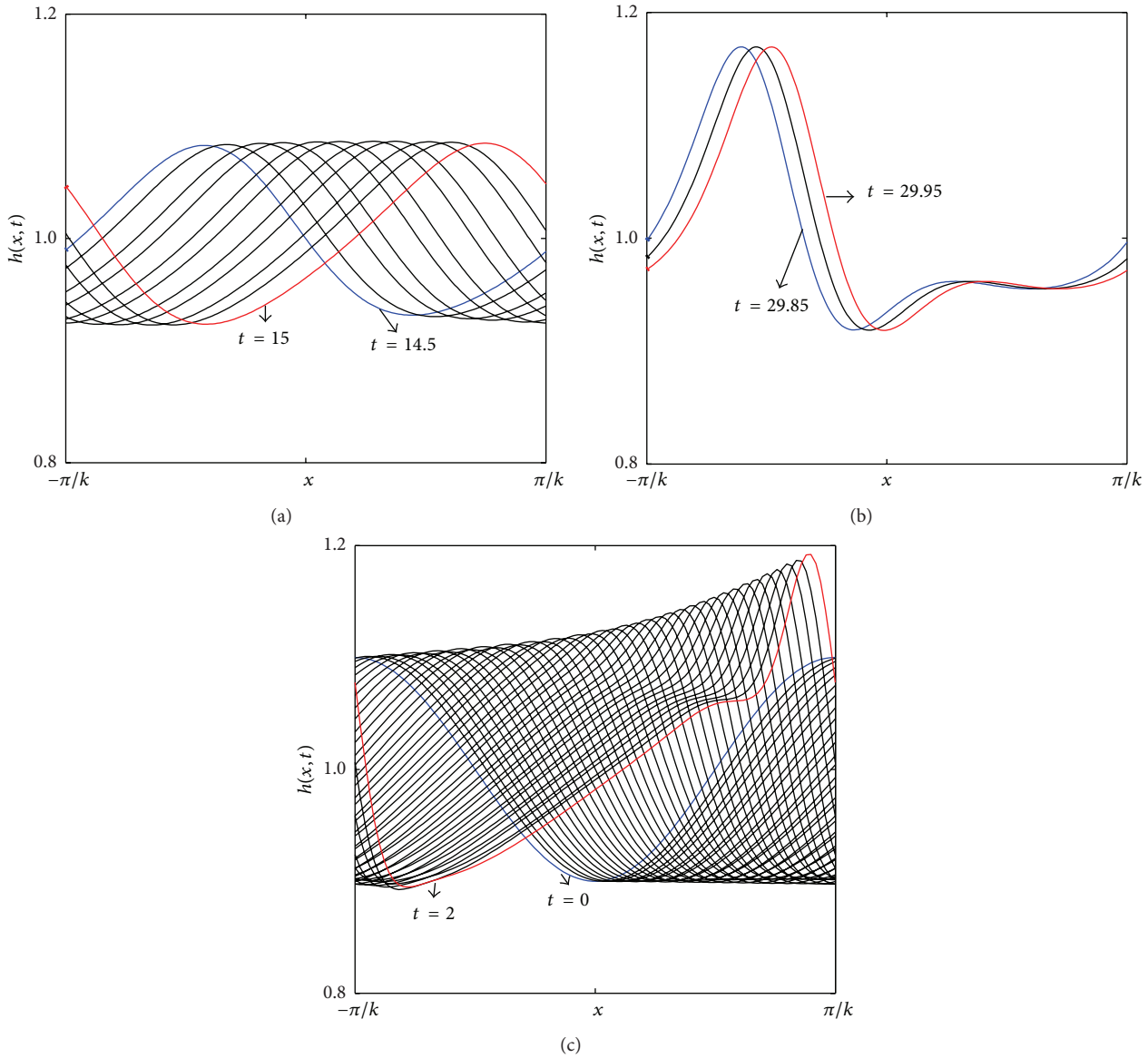

FIGURE 10: (a), (b), and (c) represent the surface-wave instability curves reproduced from Joo et al. [7] corresponding to Figures 5(b), 7(a), and 9(a), respectively, in their study.

If m_1^* and m_2^* are the fixed points obtained from (35) and (36), the stability or instability of the fixed points corresponding to traveling waves depends on the sign of the eigenvalues of the following matrix:

$$J = \begin{pmatrix} 2\alpha^2 b_{131} m_1^{*2} & \alpha^2 \varphi_1 m_1^* & -\alpha^2 \sin\phi^* \left(b_{121} + \dfrac{c_{121} b_{221}}{c_{221}} \right) m_1^* m_2^* \\ 2\left(\varphi_2 + \alpha^2 b_{231} m_2^* \right) m_1^* & \alpha^2 b_{211} m_1^{*2} & 0 \\ 2\alpha^2 k A_1'' m_1^* & -2\alpha^2 \left(b_{121} + \dfrac{c_{121} b_{221}}{c_{221}} \right) \sin\phi^* & -\left(2\alpha^2 \varphi_1 m_2^* + \varphi_2 \dfrac{m_1^{*2}}{m_2^*} \right) \end{pmatrix}. \tag{38}$$

6. Nonlinear Development of the Interfacial Surface

The nonlinear interactions are studied numerically beyond the linear stability threshold in a periodic domain, $\mathbb{D} = \{(x,t) : x \in (-\pi/k_m, \pi/k_m), t \in [0,\infty)\}$, by solving (10) subject to the initial condition $h(x,0) = 1 - 0.1\cos(k_m x)$. A central difference scheme, which is second-order accurate in space, and a backward Euler method, which is implicit in forward time, are adopted to solve the problem in MATLAB.

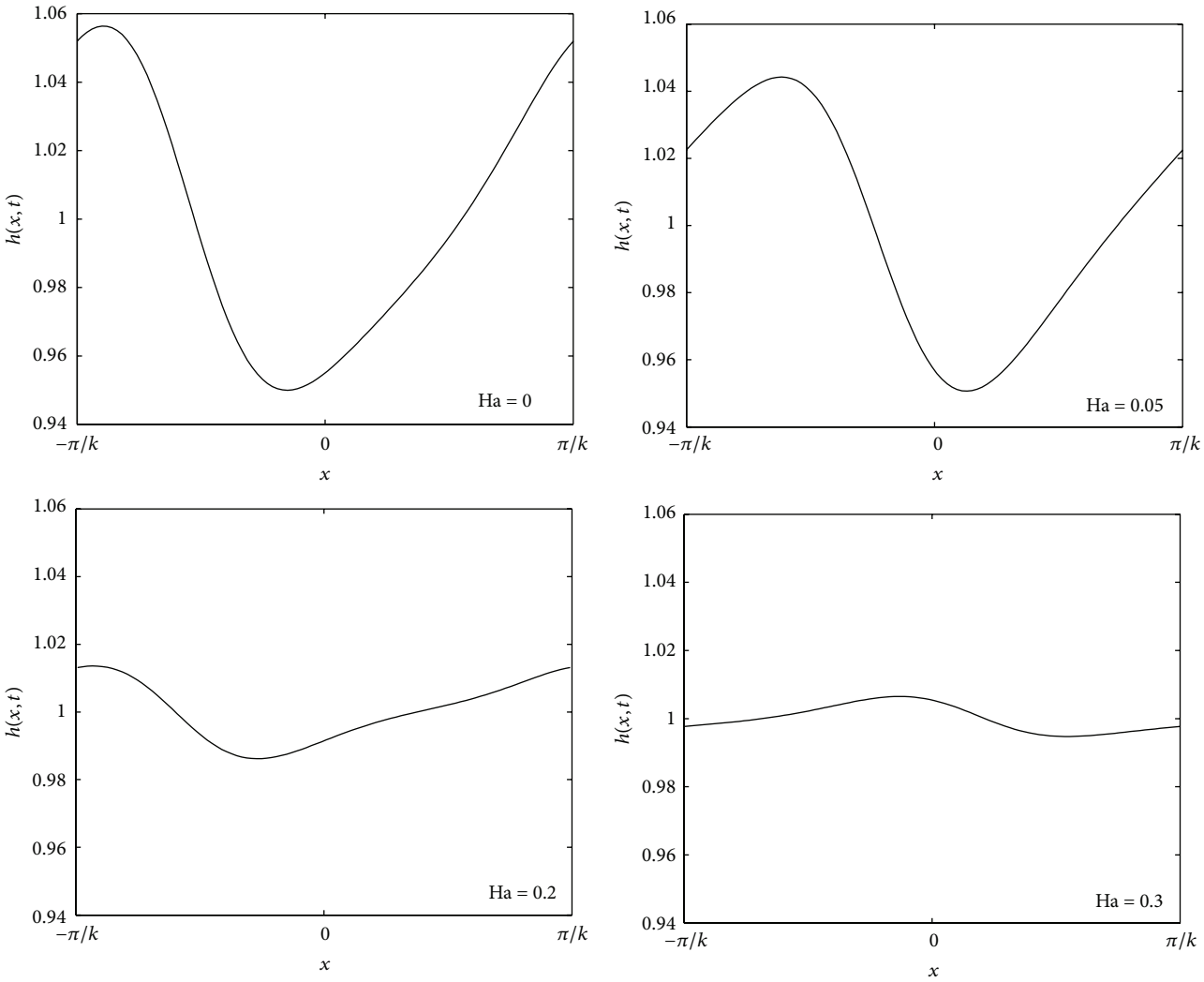

Figure 11: Free surface profiles at Re = 5, $\beta = 45^{\circ}$, and $S = 5$ when $\tau = 0$ at time $t = 250$.

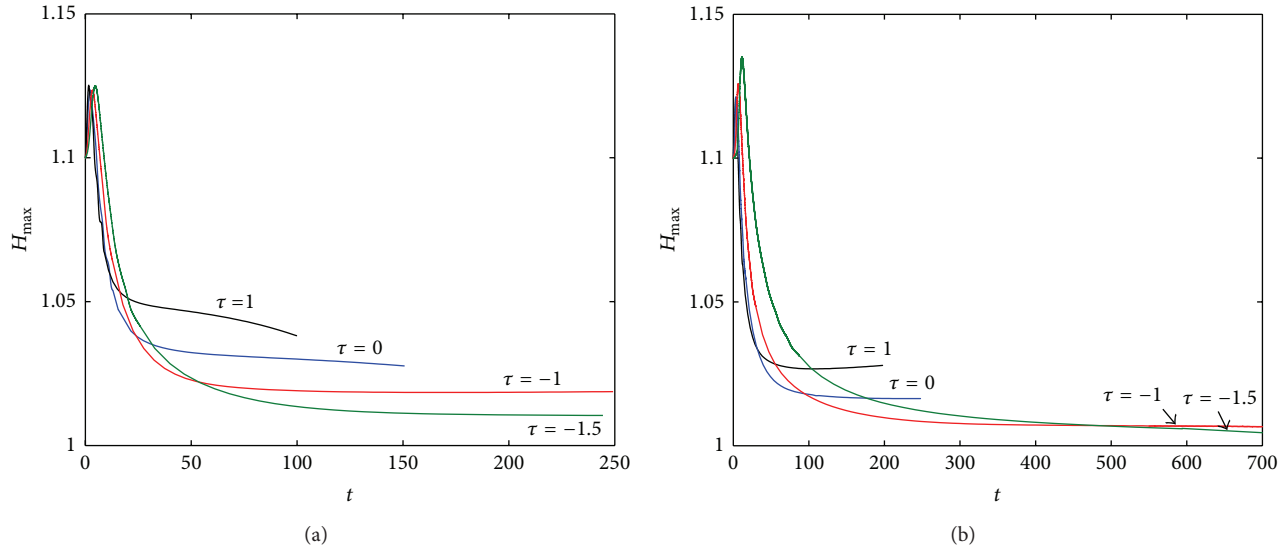

Figure 12: Maximum film thickness profiles at Re = 5, $\beta = 45^{\circ}$, and $S = 5$: (a) Ha = 0.05 and (b) Ha = 0.2.

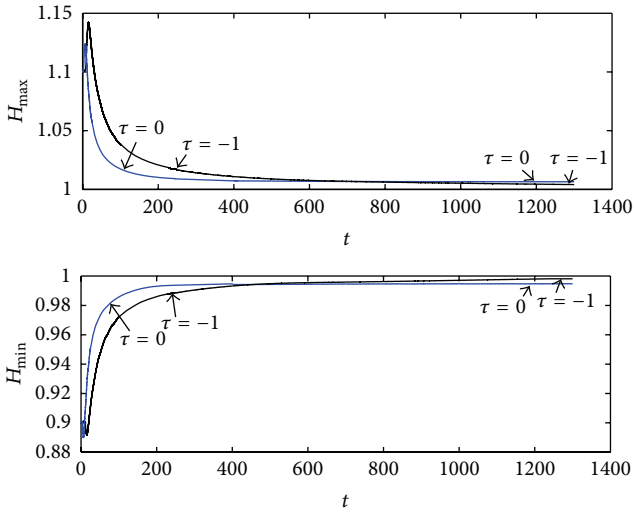

FIGURE 13: Maximum and minimum amplitude profiles corresponding to Re = 5, $\beta = 45^{\circ}$, $S = 5$, and Ha = 0.3.

The local truncation error for this numerical scheme is $\mathcal{T} = \mathcal{O}(\Delta t, \Delta x^2)$. The computations are performed with a small time increment, $\Delta t = 10^{-3}$. The numerical scheme is always stable (since a backward Euler method is used) and does not build up errors. The number of nodes along the spatial direction is $N = 800$ such that the spatial step length is $\Delta x = 2\pi/Nk_m$. An error tolerance of 10^{-10} is set, and the simulations are stopped once the absolute value of the error becomes smaller than this value. Also, the numerical simulations show no particular deviation from the results obtained neither when the spatial grid points are doubled nor when the time step is further reduced. Figures 5(b), 7(a), and 9(a) available in Joo et al. [7] are reproduced in Figure 10 to show the correctness of the numerical scheme. This gives confidence in applying it to the evolution equation considered here.

The effect of the transverse magnetic field is illustrated in Figure 11. The wave structure when the magnetic field strength is zero displays a steep curvier wave than when Ha > 0. The surface-wave instability decreases when the strength of the applied magnetic field increases. This reveals the stabilizing mechanism of the transversely applied magnetic field.

Figure 12 displays maximum amplitude profiles of the sheared flow for two different values of Ha on a semi-inclined plane. The maximum amplitude initially increases and then decreases. Due to saturation of the nonlinear interactions, the initial perturbation of the free surface is damped after a long time. For a short time, the amplitude profile corresponding to $\tau > 0$ remains smaller than the ones corresponding to $\tau \leq 0$. Also, for different Ha, the amplitudes corresponding to $\tau < 0$ remain larger than those corresponding to $\tau = 0$ up to a certain time (see also Figure 13). However, these trends change over time. When the magnitude of the Hartmann number increases, the time required for the amplitudes corresponding to $\tau < 0$ to decrease below the amplitude corresponding to $\tau = 0$ increases (Figures 12(a), 12(b), and 13). In addition, it is also observed that the time needed for the amplitude profiles corresponding to $\tau = -1$ to dominate the amplitude profiles corresponding to $\tau = -1.5$ increases when the value of Ha increases (Figures 12(a) and 12(b)).

The surface waves emerging at the free surface are captured and presented in Figure 14. For $\tau = 0$, a wave which has a stretched front is observed after a long time. When $\tau = -1$, a one-humped solitary-like wave is formed when a large amplitude wave and a small capillary ripple coalesce together (Figure 14(b)) at the time of saturation (a certain time after which all of the waves have the same structure and shape). Figure 14 demonstrates that the instability measured by the wave height decreases when the shear is induced along the uphill direction.

Tsai et al. [28] pointed out that, when the intensity of the magnetic field increases, the flow retards and stabilizes the system. The interfacial surface subjected to air shear affects the velocity and flow rate, $q(x,t) = \int_0^h u(x,t)dy$, for different values of τ and Ha (Figure 15). The numerical interactions reveal that the velocity and the flow rate can either increase or decrease depending on the direction the air shears the deformable free interface. In conjunction to the nonlinear wave speed traced in Figure 8, the velocity profiles traced in Figure 15 show a similar response. For Ha = 0 and $\tau > 0$, the streamwise velocity and the flow rate increase. Also, the transverse velocity is larger for Ha = 0 than when Ha > 0. Furthermore, the velocity and the flow rate decrease when the strength of the applied magnetic field increases. When the magnitude of the shear induced in the uphill direction is increased (by considering a small negative τ value) for large values of Ha, constant velocity and flow rate profiles are observed.

It is inferred from the nonlinear simulations that the effect of magnetic field and wind shear greatly affects the thickness of the interfacial free surface. When the strength of the magnetic field increases, the flow has a uniform velocity and constant discharge. For Ha > 0, the transverse velocity shows a small growth in the positive direction. The growth of the unwanted development of the free surface is retarded by the magnetic field, when it acts opposite to the flow direction. Such a growth-reducing mechanism of the amplitude, in particular, can be further enhanced by applying uphill shear on the free surface. This inclusion causes further reduction in the values of streamwise and transverse velocities, thereby leading to constant flux situation and improved stability.

7. Conclusions and Perspectives

Linear and nonlinear analyses on the stability of a thin film subjected to air shear on a free surface in the presence of a transversely applied external magnetic field of constant strength have been studied. Instead of obtaining the solutions at different orders of approximation using a power series approach [37–39, 43], the solutions of equations arising at various orders have been straightforwardly solved [28].

The linear stability results gave firsthand information about the stability mechanism. The modal interaction

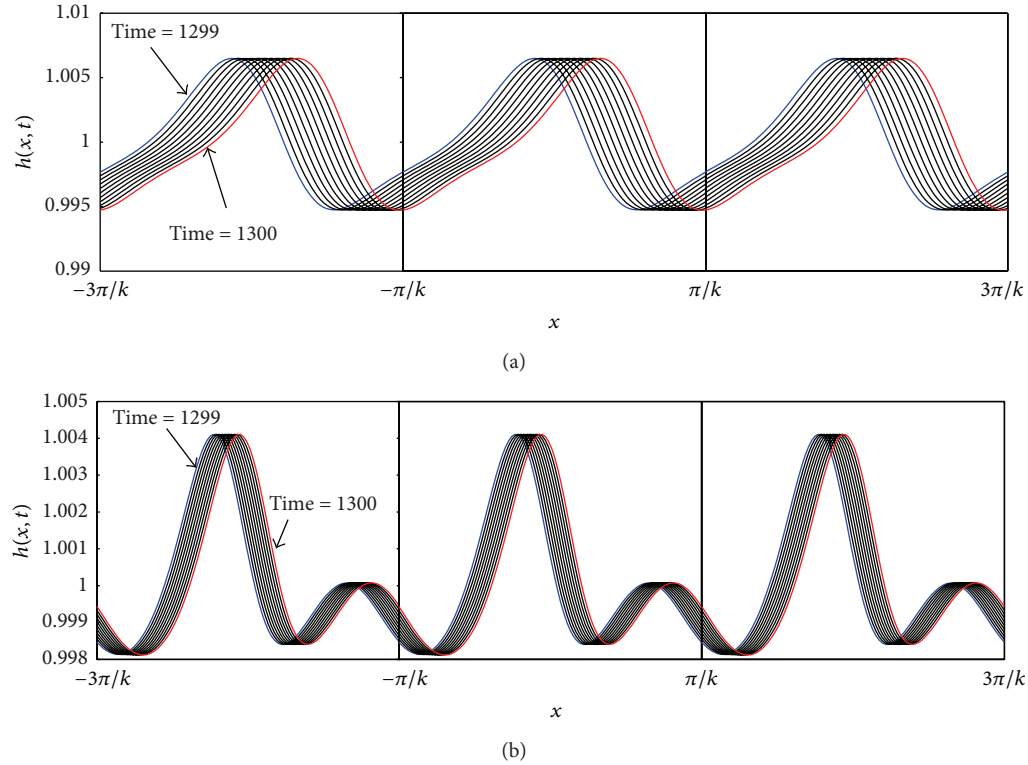

FIGURE 14: Evolution of the surface-wave instability at Re = 5, $\beta = 45^{\circ}$, $S = 5$, and Ha = 0.3: (a) $\tau = 0$ and (b) $\tau = -1$. The waves are plotted at a gap of 0.1 time units in a periodic domain.

phenomenon was studied by deriving a complex Ginzburg-Landau-type equation using the method of multiple scales. The stability regimes identified by the linear theory were further categorized using the weakly nonlinear theory by considering a filtered wave to be the solution of the complex Ginzburg-Landau equation. When the nonlinear amplification rate (J_2) is positive, an infinitesimal disturbance in the linearly unstable region attains a finite-amplitude equilibrium state. The threshold amplitude and the nonlinear wave speed exist in the supercritical stable region. Stability of a filtered wave subject to sideband disturbances was considered, and the conditions under which the eigenvalues decay in time were mathematically identified. Considering the initial thickness to be one and imposing restrictions upon the amplitude coefficients, a truncated Fourier series was used to derive a bimodal dynamical system. The stability of the pure-mode, mixed-mode, and the traveling wave solution has been mathematically discussed.

Although there are several investigations based on weakly nonlinear theory [28, 37–40, 43], the complete nonlinear evolution equation was not studied numerically beyond the linear stability threshold in the presence of an external magnetic field, especially in a short-circuited system. In this regard, the nonlinear interactions have been numerically assessed using finite-difference technique with an implicit time-stepping procedure. Using such a scheme, the evolution of disturbances to a small monochromatic perturbation was analyzed. The destabilizing mechanism of the downhill shear was identified with the help of computer simulation. Also, it takes a long time for the amplitude profiles corresponding to the zero-shear-induced effect to dominate those corresponding to the uphill shear, when the strength of the magnetic field increases. Furthermore, among the uphill shear-induced flows, the smaller the uphill shear-induced effect is, the longer it takes for the respective amplitude to be taken over by the amplitude corresponding to large values of uphill shear, provided that the magnetic fields intensity increases.

The velocity and the flow rate profiles gave a clear understanding of the physical mechanism involved in the process. When the magnetic field effect and the air shear are not considered, the gravitational acceleration, the inertial force, and the hydrostatic pressure determine the mechanism of long-wave instability, by competing against each other. These forces trigger the flow, amplify the film thickness, and prevent the wave formation, respectively [66]. When the magnetic field effect is included, it competes with other forces to decide the stability threshold. The applied magnetic field retards the flow considerably by reducing the transverse velocity. This phenomenon reduces the wave thickness, but it favors hydrostatic pressure and surface-tension to promote stability on a semi-inclined plane. However, when the air shear is considered, it can either stabilize or destabilize the system depending on the direction it shears the free surface. For downhill shear, the transverse velocity increases

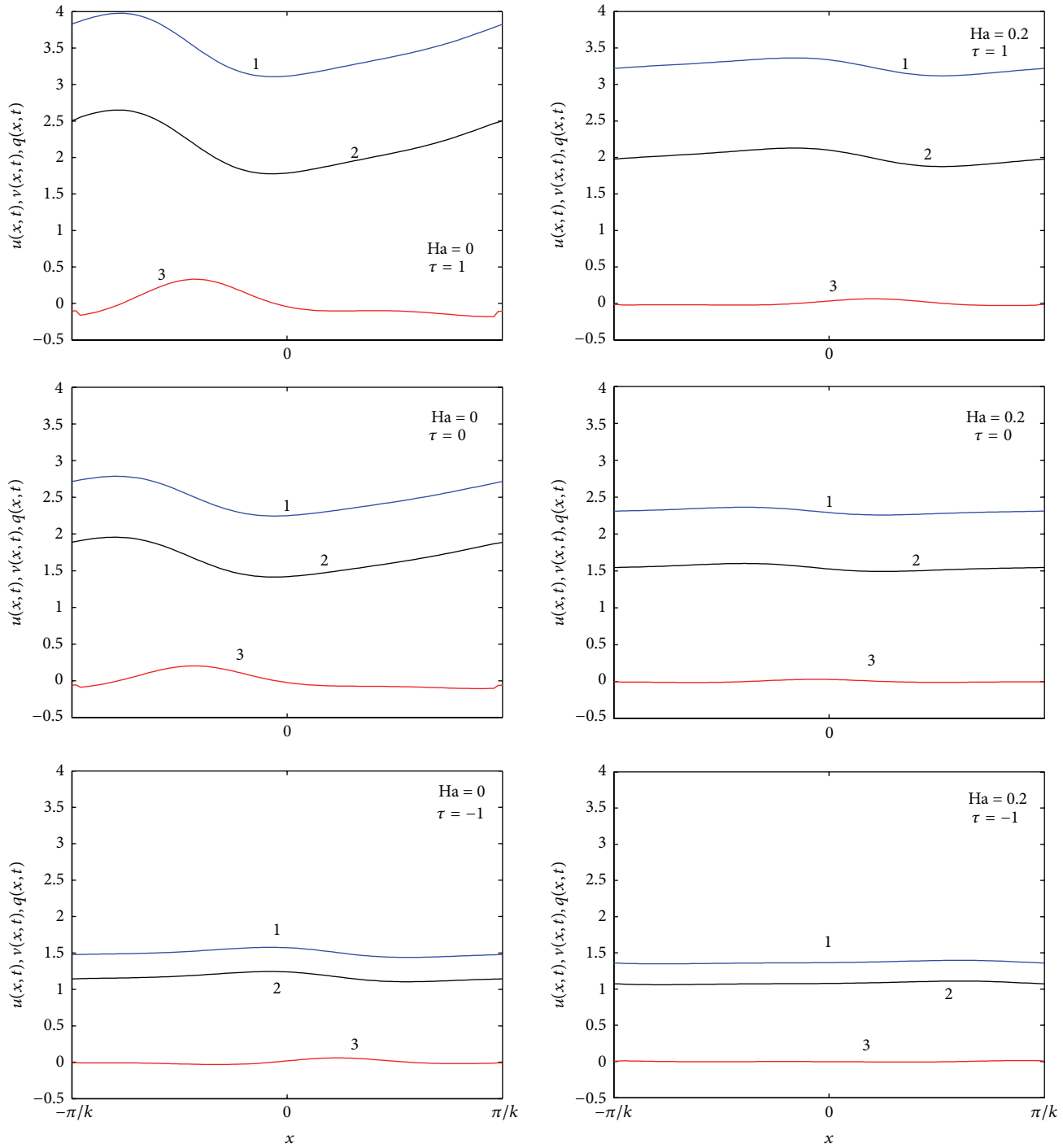

Figure 15: (1) Streamwise velocity, (2) flow rate, and (3) transverse velocity profiles at Re = 5, $\beta = 45^{\circ}$, and $S = 5$ in a periodic domain.

resulting in increased accumulation of the fluid under a typical cusp, thereby favoring inertial force. Overall, this mechanism causes the film thickness to increase. For uphill shear, the results are opposite.

The present investigation suggests the inclusion of superficial shear stress on the interfacial surface to enhance the stability of the film, or on the other hand, shows the natural effect of air shear on the films stability under natural conditions, in particular to those films subjected to a transversely applied uniform external magnetic field in a short-circuited system. Future research activities may include (i) assessing nonisothermal effects, (ii) studying non-Newtonian films, and (iii) considering the contribution of electric field. The last point would demand considering Poisson equation to

describe electric potential together with appropriate boundary conditions.

Appendices

A. Dimensionless Equations

The dimensionless equations are given by

$$u_x + v_y = 0,$$
$$\varepsilon\left(u_t + uu_x + vu_y\right) = -\varepsilon p_x + \varepsilon^2 u_{xx} + u_{yy} + \mathrm{Re} - \mathrm{Ha}u, \quad \text{(A.1)}$$
$$\varepsilon^2\left(v_t + uv_x + vv_y\right) = -p_y + \varepsilon^3 v_{xx} + \varepsilon v_{yy} - \mathrm{Re}\,\cot\beta,$$

and the respective boundary conditions are

$$u = 0, \qquad v = 0 \quad \text{on} \quad y = 0, \quad \text{(A.2)}$$

$$p + 2\varepsilon\frac{\left(1-\varepsilon^2 h_x^2\right)}{\left(1+\varepsilon^2 h_x^2\right)}u_x + \frac{2\varepsilon h_x}{1+\varepsilon^2 h_x^2}\left(u_y + \varepsilon^2 v_x\right) = -\frac{\varepsilon^2\,\overline{S}\,h_{xx}}{\left(1+\varepsilon^2 h_x^2\right)^{3/2}} \quad \text{on} \quad y = h, \quad \text{(A.3)}$$

$$\frac{\left(1-\varepsilon^2 h_x^2\right)}{\left(1+\varepsilon^2 h_x^2\right)}\left(u_y + \varepsilon^2 v_x\right) - \frac{4\varepsilon^2 h_x}{\left(1+\varepsilon^2 h_x^2\right)}u_x = \tau \quad \text{on} \quad y = h, \quad \text{(A.4)}$$

$$v = h_t + uh_x \quad \text{on} \quad y = h. \quad \text{(A.5)}$$

B. Multiple Scale Analysis

The film thickness, H, is expanded as

$$H\left(\varepsilon, x, x_1, t, t_1, t_2\right) = \sum_{i=1}^{\infty}\alpha^i H_i\left(\varepsilon, x, x_1, t, t_1, t_2\right). \quad \text{(B.1)}$$

Exploiting (16) using (20) and (B.1), the following equation is obtained:

$$\left(L_0 + \alpha L_1 + \alpha^2 L_2\right)\left(\alpha H_1 + \alpha^2 H_2 + \alpha^3 H_3\right) = -\alpha^2 N_2 - \alpha^3 N_3, \quad \text{(B.2)}$$

where the operators L_0, L_1, and L_2 and the quantities N_2 and N_3 are given as follows

$$L_0 = \frac{\partial}{\partial t} + A_1\frac{\partial}{\partial x} + \varepsilon B_1\frac{\partial^2}{\partial x^2} + \varepsilon C_1\frac{\partial^4}{\partial x^4}, \quad \text{(B.3a)}$$

$$L_1 = \frac{\partial}{\partial t_1} + A_1\frac{\partial}{\partial x_1} + 2\varepsilon B_1\frac{\partial^2}{\partial x\partial x_1} + 4\varepsilon C_1\frac{\partial^4}{\partial x^3\partial x_1}, \quad \text{(B.3b)}$$

$$L_2 = \frac{\partial}{\partial t_2} + \varepsilon B_1\frac{\partial^2}{\partial x_1^2} + 6\varepsilon C_1\frac{\partial^4}{\partial x^2\partial x_1^2}, \quad \text{(B.3c)}$$

$$N_2 = A_1' H_1 H_{1x} + \varepsilon B_1' H_1 H_{1xx} + \varepsilon C_1' H_1 H_{1xxxx} + \varepsilon B_1' H_{1x}^2 + \varepsilon C_1' H_{1x} H_{1xxx}, \quad \text{(B.3d)}$$

$$\begin{aligned} N_3 = {} & A_1'\left(H_1 H_{2x} + H_1 H_{1x_1} + H_2 H_{1x}\right) \\ & + \varepsilon B_1'\left(H_1 H_{2xx} + 2H_1 H_{1xx_1} + H_2 H_{1xx}\right) \\ & + \varepsilon C_1'\left(H_1 H_{2xxxx} + 4H_1 H_{1xxxx_1} + H_2 H_{1xxxx}\right) \\ & + \varepsilon B_1'\left(2H_{1x} H_{2x} + 2H_{1x} H_{1x_1}\right) \\ & + \varepsilon C_1'\left(H_{2xxx} H_{1x} + 3H_{1xxx_1} H_{1x} + H_{1xxx} H_{2x} + H_{1xxx} H_{1x_1}\right) \\ & + \frac{A_1''}{2} H_1^2 H_{1x} + \varepsilon\frac{B_1''}{2} H_1^2 H_{1xx} + \varepsilon\frac{C_1''}{2} H_1^2 H_{1xxxx} \\ & + \varepsilon B_1'' H_1 H_{1x}^2 + \varepsilon C_1'' H_1 H_{1x} H_{1xxx}. \end{aligned} \quad \text{(B.3e)}$$

The equations are solved order-by-order up to $O(\alpha^3)$ [12, 14, 56, 57] to arrive at an equation related to the complex Ginzburg-Landau type for the perturbation amplitude $\eta(x_1, t_1, t_2)$:

$$\frac{\partial\eta}{\partial t_2} - \alpha^{-2} C_R\eta + \varepsilon\left(B_1 - 6k^2 C_1\right)\frac{\partial^2\eta}{\partial x_1^2} + \left(J_2 + iJ_4\right)|\eta|^2\eta = 0, \quad \text{(B.4)}$$

where

$$\begin{aligned} e_r &= \frac{2\left(B_1' - k^2 C_1'\right)}{\left(-4B_1 + 16k^2 C_1\right)}, \qquad e_i = \frac{-A_1'}{\varepsilon\left(-4kB_1 + 16k^3 C_1\right)}, \\ J_2 &= \varepsilon\left(7k^4 e_r C_1' - k^2 e_r B_1' - \frac{k^2}{2}B_1'' + \frac{k^4}{2}C_1''\right) - ke_i A_1', \\ J_4 &= \varepsilon\left(7k^4 e_i C_1' - k^2 e_i B_1'\right) + ke_r A_1' + k\frac{A_1''}{2}. \end{aligned} \quad \text{(B.5)}$$

It should be remarked that in (B.4) an imaginary, apparently convective term of the form

$$iv\frac{\partial\eta}{\partial x_1} = 2ik\varepsilon\left(B_1 - 2k^2 C_1\right)\alpha^{-1}\frac{\partial\eta}{\partial x_1} \quad \text{(B.6)}$$

could be additionally considered on the left-hand side of (B.4) as done in Dandapat and Samanta [12] and Samanta [65], provided that such a term is of $\mathcal{O}(\alpha)$ and $v < 0$. Such a term arises in the secular condition at $O(\alpha^3)$ as a contribution arising from one of the terms from $L_1 H_1$ at $O(\alpha^2)$. The solution of (B.4) for a filtered wave in which the spatial modulation does not exist and the diffusion term in (B.4) becomes zero is obtained by considering $\eta = \Gamma_0(t_2)e^{[-ib(t_2)t_2]}$.

This leads to a nonlinear ordinary differential equation for Γ_0, namely,

$$\frac{d\Gamma_0}{dt_2} - i\Gamma_0 \frac{d}{dt_2}\left[b\left(t_2\right)t_2\right] - \alpha^{-2}C_R\Gamma_0 + \left(J_2 + iJ_4\right)\Gamma_0^3 = 0, \tag{B.7}$$

where the real and imaginary parts, when separated from (37), give

$$\frac{d\left[\Gamma_0\left(t_2\right)\right]}{dt_2} = \left(\alpha^{-2}C_R - J_2\Gamma_0^2\right)\Gamma_0, \tag{B.8}$$

$$\frac{d\left[b\left(t_2\right)t_2\right]}{dt_2} = J_4\Gamma_0^2. \tag{B.9}$$

If $J_2 = 0$ in (B.8), the Ginzburg-Landau equation is reduced to a linear ordinary differential equation for the amplitude of a filtered wave. The second term on the right-hand side in (B.8) induced by the effect of nonlinearity can either accelerate or decelerate the exponential growth of the linear disturbance depending on the signs of C_R and J_2. The perturbed wave speed caused by the infinitesimal disturbances appearing in the nonlinear system can be modified using (B.8). The threshold amplitude $\alpha\Gamma_0$ from (B.8) is obtained as (when Γ_0 is nonzero and independent of t_2)

$$\alpha\Gamma_0 = \sqrt{\frac{C_R}{J_2}}. \tag{B.10}$$

Equation (B.9) with the use of (B.10) gives

$$b = \frac{C_R J_4}{\alpha^2 J_2}. \tag{B.11}$$

The speed N_c of the nonlinear wave is now obtained from (26) by substituting $\eta = \Gamma_0 e^{[-ibt_2]}$ and by using $t_2 = \alpha^2 t$. This gives the nonlinear wave speed as

$$N_c = C_{LV} + \alpha^2 b = C_{LV} + C_R\frac{J_4}{J_2}. \tag{B.12}$$

C. Sideband Stability

The sideband instability is analyzed by subjecting $\Gamma_s(t_2)$ to sideband disturbances in the form of ($\Delta \ll 1$) [12, 56, 57]

$$\eta = \Gamma_s\left(t_2\right) + \left(\Delta\Gamma_+\left(t_2\right)e^{ikx} + \Delta\Gamma_-\left(t_2\right)e^{-ikx}\right)e^{-ibt_2}, \tag{C.1}$$

in (B.4). Neglecting the nonlinear terms and separating the coefficients of $\Delta e^{i(kx-bt_2)}$ and $\Delta e^{-i(kx-bt_2)}$, the following set of equations are derived ($v = (2\varepsilon k/\alpha)(B_1 - 2k^2C_1) < 0$, $c_i = \alpha^{-2}C_R$, and $J_{1r} = \varepsilon(B_1 - 6k^2C_1) < 0$ since $B_1 - k^2C_1 = \mathcal{O}(\alpha^2)$):

$$\frac{d\Gamma_+\left(t_2\right)}{dt_2} = \left(i\mathscr{P} + kv + c_i + k^2J_{1r} - 2\left(J_2 + iJ_4\right)\left|\Gamma_s\right|^2\right) \times \Gamma_+\left(t_2\right) - \left(J_2 + iJ_4\right)\left|\Gamma_s\right|^2\overline{\Gamma}_-\left(t_2\right), \tag{C.2a}$$

$$\frac{d\Gamma_-\left(t_2\right)}{dt_2} = \left(i\mathscr{P} - kv + c_i + k^2J_{1r} - 2\left(J_2 + iJ_4\right)\left|\Gamma_s\right|^2\right) \times \Gamma_-\left(t_2\right) - \left(J_2 + iJ_4\right)\left|\Gamma_s\right|^2\overline{\Gamma}_+\left(t_2\right), \tag{C.2b}$$

where the barred quantities are the complex conjugates corresponding to their counterparts. For convenience, the above system is represented as

$$\begin{pmatrix} \dfrac{d\Gamma_+\left(t_2\right)}{dt_2} \\ \dfrac{d\overline{\Gamma}_-\left(t_2\right)}{dt_2} \end{pmatrix} = \mathscr{M}\begin{pmatrix} \Gamma_+\left(t_2\right) \\ \overline{\Gamma}_-\left(t_2\right) \end{pmatrix}, \tag{C.3}$$

where $\mathscr{M}$ is a 2×2 matrix whose entries are

$$\begin{aligned} M_{11} &= i\mathscr{P} + kv + c_i + k^2J_{1r} - 2\left(J_2 + iJ_4\right)\left|\Gamma_s\right|^2, \\ M_{22} &= -i\mathscr{P} - kv + c_i + k^2J_{1r} - 2\left(J_2 - iJ_4\right)\left|\Gamma_s\right|^2, \\ M_{12} &= -\left(J_2 + iJ_4\right)\left|\Gamma_s\right|^2, \qquad M_{21} = \overline{M}_{12}. \end{aligned} \tag{C.4}$$

Setting $\Gamma_+(t_2) \propto e^{\vartheta t_2}$ and $\overline{\Gamma}_-(t_2) \propto e^{\vartheta t_2}$, the eigenvalues are obtained from $|\mathscr{M} - \vartheta I| = 0$, and the stability of (22) subject to sideband disturbances as $t_2 \to \infty$ demands that $\vartheta < 0$. The eigenvalues are found as follows

$$\vartheta = \frac{1}{2}\left(\operatorname{tr}\left(\mathscr{M}\right) \pm \sqrt{\operatorname{tr}^2\left(\mathscr{M}\right) - 4\det\left(\mathscr{M}\right)}\right). \tag{C.5}$$

D. Bimodal Dynamical System

In order to analyze the stability of the bimodal dynamical system, the film thickness is expanded as a truncated Fourier series ($z_n(t)$ is complex, and a bar above it designates its complex conjugate)

$$h\left(x,t\right) = 1 + \sum_{n=1}^{2} z_n\left(t\right)e^{nikx} + \overline{z}_n\left(t\right)e^{-nikx} \tag{D.1}$$

and is substituted in the evolution equation (10). A Taylor series expansion is then sought to be about "1", and the

following coupled dynamical system is obtained from the coefficients of e^{ikx} and e^{2ikx} terms:

$$\frac{d}{dt}z_1(t) = a_{111}z_1(t) + a_{121}\overline{z}_1(t)\,z_2(t) + z_1(t)\left(a_{131}|z_1|^2 + a_{132}|z_2|^2\right), \tag{D.2a}$$

$$\frac{d}{dt}z_2(t) = a_{211}z_2(t) + a_{221}z_1^2(t) + z_2(t)\left(a_{231}|z_1|^2 + a_{232}|z_2|^2\right). \tag{D.2b}$$

It should be remarked that the higher-order terms arising while deducing (D.2a) and (D.2b) are neglected by assuming that $|z_1| \ll 1$ and $|z_2| \ll |z_1|$. The coefficients of the above system are given by

$$\begin{aligned}
a_{111} &= \varepsilon\left(k^2B_1 - k^4C_1\right) - ikA_1,\\
a_{211} &= \varepsilon\left(4k^2B_1 - 16k^4C_1\right) - 2ikA_1,\\
a_{121} &= \varepsilon\left(k^2B_1' - 7k^4C_1'\right) - ikA_1',\\
a_{221} &= \varepsilon\left(2k^2B_1' - 2k^4C_1'\right) - ikA_1',\\
a_{131} &= \frac{\varepsilon}{2}\left(k^2B_1'' - k^4C_1''\right) - \frac{i}{2}kA_1'',\\
a_{231} &= \varepsilon\left(4k^2B_1'' - 16k^4C_1''\right) - 2ikA_1'',\\
a_{132} &= \varepsilon\left(k^2B_1'' - k^4C_1''\right) - ikA_1'',\\
a_{232} &= \varepsilon\left(2k^2B_1'' - 8k^4C_1''\right) - ikA_1''.
\end{aligned} \tag{D.3}$$

The complex conjugates occurring in system (D.3) can be avoided by representing $z_n(t) = a_n(t)e^{i\theta_n(t)}$ in polar form, where $a_n(t)$ and $\theta_n(t)$ are real functions such that $n = 1, 2$. Using polar notation, the following three equations are obtained:

$$\begin{aligned}
\frac{da_1(t)}{dt} &= f_1\left(a_1(t), a_2(t), \phi(t)\right)\\
&= b_{111}a_1(t) + \left[b_{121}\cos\phi(t) + c_{121}\sin\phi(t)\right]\\
&\quad \times a_1(t)\,a_2(t) + a_1(t)\left[b_{131}a_1^2(t) + b_{132}a_2^2(t)\right],
\end{aligned} \tag{D.4a}$$

$$\begin{aligned}
\frac{da_2(t)}{dt} &= f_2\left(a_1(t), a_2(t), \phi(t)\right)\\
&= b_{211}a_2(t) + \left[b_{221}\cos\phi(t) - c_{221}\sin\phi(t)\right]\\
&\quad \times a_1^2(t) + a_2(t)\left[b_{231}a_1^2(t) + b_{232}a_2^2(t)\right],
\end{aligned} \tag{D.4b}$$

$$\begin{aligned}
\frac{d\phi(t)}{dt} &= f_3\left(a_1(t), a_2(t), \phi(t)\right)\\
&= kA_1''\left(a_1^2 - a_2^2\right) + 2\left[c_{121}\cos\phi(t) - b_{121}\sin\phi(t)\right]\\
&\quad \times a_2(t) - \left[b_{221}\sin\phi(t) + c_{221}\cos\phi(t)\right]\frac{a_1^2(t)}{a_2(t)}.
\end{aligned} \tag{D.4c}$$

While the coefficient of $e^{i\theta_n(t)}$ term yields (D.4a) and (D.4b), (D.4c) is obtained from the two equations which result as the coefficient of $ie^{i\theta_n(t)}$ term with the imposition that the phase relationship is defined as $\phi(t) = 2\theta_1(t) - \theta_2(t)$. The terms b_{ijk} and c_{ijk} are real numbers and represent the real and imaginary parts of a typical a_{ijk} term in (D.3) such that $i, k = 1, 2$ and $j = 1, 2, 3$.

References

[1] D. J. Benney, "Long waves on liquid films," *Journal of Mathematical Physics*, vol. 45, pp. 150–155, 1966.

[2] B. Gjevik, "Occurrence of finite-amplitude surface waves on falling liquid films," *Physics of Fluids*, vol. 13, no. 8, pp. 1918–1925, 1970.

[3] R. W. Atherton and G. M. Homsy, "On the derivation of evolution equations for interfacial waves," *Chemical Engineering Communications*, vol. 2, no. 2, pp. 57–77, 1976.

[4] S. P. Lin and M. V. G. Krishna, "Stability of a liquid film with respect to initially finite three-dimensional disturbances," *Physics of Fluids*, vol. 20, no. 12, pp. 2005–2011, 1977.

[5] A. Pumir, P. Manneville, and T. Pomeau, "On solitary waves running down an inclined plane," *Journal of Fluid Mechanics*, vol. 135, pp. 27–50, 1983.

[6] J. P. Burelbach, S. G. Bankoff, and S. H. Davis, "Nonlinear stability of evaporating/condensing liquid films," *Journal of Fluid Mechanics*, vol. 195, pp. 463–494, 1988.

[7] S. W. Joo, S. H. Davis, and S. G. Bankoff, "Long-wave instabilities of heated falling films. Two-dimensional theory of uniform layers," *Journal of Fluid Mechanics*, vol. 230, pp. 117–146, 1991.

[8] S. W. Joo and S. H. Davis, "Instabilities of three-dimensional viscous falling films," *Journal of Fluid Mechanics*, vol. 242, pp. 529–547, 1992.

[9] S. Miladinova, S. Slavtchev, G. Lebon, and J.-C. Legros, "Long-wave instabilities of non-uniformly heated falling films," *Journal of Fluid Mechanics*, vol. 453, pp. 153–175, 2002.

[10] S. Miladinova, D. Staykova, G. Lebon, and B. Scheid, "Effect of nonuniform wall heating on the three-dimensional secondary instability of falling films," *Acta Mechanica*, vol. 156, no. 1-2, pp. 79–91, 2002.

[11] B. Scheid, A. Oron, P. Colinet, U. Thiele, and J. C. Legros, "Nonlinear evolution of nonuniformly heated falling liquid films," *Physics of Fluids*, vol. 15, no. 2, p. 583, 2003, Erratum in: Physics of Fluids, vol. 14, pp. 4130, 2002.

[12] B. S. Dandapat and A. Samanta, "Bifurcation analysis of first and second order Benney equations for viscoelastic fluid flowing down a vertical plane," *Journal of Physics D*, vol. 41, no. 9, Article ID 095501, 2008.

[13] R. Usha and I. M. R. Sadiq, "Weakly nonlinear stability analysis of a non-uniformly heated non-Newtonian falling film," in *Proceedings of the 5th Joint ASME/JSME Fluids Engineering Summer Conference (FEDSM '07)*, pp. 1661–1670, August 2007.

[14] I. M. R. Sadiq and R. Usha, "Thin Newtonian film flow down a porous inclined plane: stability analysis," *Physics of Fluids*, vol. 20, no. 2, Article ID 022105, 2008.

[15] I. M. R. Sadiq and R. Usha, "Effect of permeability on the instability of a non-Newtonian film down a porous inclined plane," *Journal of Non-Newtonian Fluid Mechanics*, vol. 165, no. 19-20, pp. 1171–1188, 2010.

[16] U. Thiele, B. Goyeau, and M. G. Velarde, "Stability analysis of thin film flow along a heated porous wall," *Physics of Fluids*, vol. 21, no. 1, Article ID 014103, 2009.

[17] I. M. R. Sadiq, R. Usha, and S. W. Joo, "Instabilities in a liquid film flow over an inclined heated porous substrate," *Chemical Engineering Science*, vol. 65, no. 15, pp. 4443–4459, 2010.

[18] B. Uma, "Effect of wind stress on the dynamics and stability of non-isothermal power-law film down an inclined plane," *ISRN Mathematical Physics*, vol. 2012, Article ID 732675, 31 pages, 2012.

[19] B. Scheid, C. Ruyer-Quil, U. Thiele, O. A. Kabov, J. C. Legros, and P. Colinet, "Validity domain of the Benney equation including the Marangoni effect for closed and open flows," *Journal of Fluid Mechanics*, vol. 527, pp. 303–335, 2005.

[20] S. Chandrasekhar, "The stability of viscous flow between rotating cylinders in the presence of a magnetic field," *Proceedings of the Royal Society of London A*, vol. 216, pp. 293–309, 1953.

[21] J. T. Stuart, "On the stability of viscous flow between parallel planes in the presence of a co-planar magnetic field," *Proceedings of the Royal Society of London A*, vol. 221, pp. 189–206, 1954.

[22] R. C. Lock, "The stability of the flow of an electrically conducting fluid between parallel planes under a transverse magnetic field," *Proceedings of the Royal Society of London A*, vol. 233, pp. 105–125, 1955.

[23] D.-Y. Hsieh, "Stability of a conducting fluid flowing down an inclined plane in a magnetic field," *Physics of Fluids*, vol. 8, no. 10, pp. 1785–1791, 1965.

[24] Y. P. Ladikov, "Flow stability of a conducting liquid flowing down an inclined plane in the presence of a magnetic field," *Fluid Dynamics*, vol. 1, no. 1, pp. 1–4, 1966.

[25] P. C. Lu and G. S. R. Sarma, "Magnetohydrodynamic gravity—capillary waves in a liquid film," *Physics of Fluids*, vol. 10, no. 11, p. 2339, 1967.

[26] Yu. N. Gordeev and V. V. Murzenko, "Wave film flows of a conducting viscous fluid film in the tangential magnetic field," *Applied Mathematics and Theoretical Physics*, vol. 3, p. 96, 1990.

[27] D. Gao and N. B. Morley, "Numerical investigation of surface disturbance on liquid metal falling film flows in a magnetic field gradient," *Magnitnaya Gidrodinamika*, vol. 40, no. 1, pp. 99–113, 2004.

[28] J.-S. Tsai, C.-I. Hung, and C.-K. Chen, "Nonlinear hydromagnetic stability analysis of condensation film flow down a vertical plate," *Acta Mechanica*, vol. 118, pp. 197–212, 1996.

[29] Y. Renardy and S. M. Sun, "Stability of a layer of viscous magnetic fluid flow down an inclined plane," *Physics of Fluids*, vol. 6, no. 10, pp. 3235–3248, 1994.

[30] H. H. Bau, J. Z. Zhu, S. Qian, and Y. Xiang, "A magneto-hydrodynamically controlled fluidic network," *Sensors and Actuators B*, vol. 88, no. 2, pp. 205–216, 2003.

[31] H. Kabbani, M. Marc, S. W. Joo, and S. Qian, "Analytical prediction of flow field in magnetohydrodynamic-based microfluidic devices," *Journal of Fluids Engineering*, vol. 130, no. 9, Article ID 091204, 6 pages, 2008.

[32] A. E. Radwan, "Hydromagnetic stability of a gas-liquid interface of coaxial cylinders," *Astrophysics and Space Science*, vol. 161, no. 2, pp. 279–293, 1989.

[33] M. C. Shen, S. M. Sun, and R. E. Meyer, "Surface waves on viscous magnetic fluid flow down an inclined plane," *Physics of Fluids A*, vol. 3, no. 3, pp. 439–445, 1991.

[34] M. H. Chang and C.-K. Chen, "Hydromagnetic stability of current-induced flow in a small gap between concentric rotating cylinders," *Proceedings of the Royal Society A*, vol. 454, no. 1975, pp. 1857–1873, 1998.

[35] S. Korsunsky, "Long waves on a thin layer of conducting fluid flowing down an inclined plane in an electromagnetic field," *European Journal of Mechanics B*, vol. 18, no. 2, pp. 295–313, 1999.

[36] A. J. Chamkha, "On two-dimensional laminar hydromagnetic fluid-particle flow over a surface in the presence of a gravity field," *Journal of Fluids Engineering, Transactions of the ASME*, vol. 123, no. 1, pp. 43–49, 2001.

[37] P.-J. Cheng and D. T. W. Lin, "Surface waves on viscoelastic magnetic fluid film flow down a vertical column," *International Journal of Engineering Science*, vol. 45, no. 11, pp. 905–922, 2007.

[38] P.-J. Cheng, "Hydromagnetic stability of a thin electrically conducting fluid film flowing down the outside surface of a long vertically aligned column," *Proceedings of the Institution of Mechanical Engineers C*, vol. 223, no. 2, pp. 415–426, 2009.

[39] P.-J. Cheng and K.-C. Liu, "Hydromagnetic instability of a power-law liquid film flowing down a vertical cylinder using numerical approximation approach techniques," *Applied Mathematical Modelling*, vol. 33, no. 4, pp. 1904–1914, 2009.

[40] C.-K. Chen and D.-Y. Lai, "Weakly nonlinear stability analysis of a thin magnetic fluid during spin coating," *Mathematical Problems in Engineering*, vol. 2010, Article ID 987891, 17 pages, 2010.

[41] S. K. Ghosh, O. A. Bég, and J. Zueco, "Hydromagnetic free convection flow with induced magnetic field effects," *Meccanica*, vol. 45, no. 2, pp. 175–185, 2010.

[42] O. A. Bég, J. Zueco, and T. B. Chang, "Numerical analysis of hydromagnetic gravity-driven thin film micropolar flow along an inclined plane," *Chemical Engineering Communications*, vol. 198, no. 3, pp. 312–331, 2011.

[43] P.-J. Cheng, K.-C. Liu, and D. T. W. Lin, "Hydromagnetic stability analysis of a film coating flow down a rotating vertical cylinder," *Journal of Mechanics*, vol. 27, no. 1, pp. 27–36, 2011.

[44] A. D. D. Craik, "Wind-generated waves in thin liquid films," *Journal of Fluid Mechanics*, vol. 26, no. 2, pp. 369–392, 1966.

[45] E. O. Tuck and J.-M. Vanden-Broeck, "Influence of surface tension on jet-stripped continuous coating of sheet materials," *AIChE Journal*, vol. 30, pp. 808–811, 1984.

[46] M. Sheintuch and A. E. Dukler, "Phase plane and bifurcation analysis of thin wavy films under shear," *AIChE Journal*, vol. 35, no. 2, pp. 177–186, 1989.

[47] G. J. Zabaras Jr, *Studies of vertical cocurrent and countercurrent annular gas-liquid flows [Ph.D. thesis]*, University of Houston, 1985.

[48] A. C. King and E. O. Tuck, "Thin liquid layers supported by steady air-flow surface traction," *Journal of Fluid Mechanics*, vol. 251, pp. 709–718, 1993.

[49] J. P. Pascal, "A two-layer model for a non-Newtonian gravity current subjected to wind shear," *Acta Mechanica*, vol. 162, no. 1–4, pp. 83–98, 2003.

[50] S. K. Wilson and B. R. Duffy, "Unidirectional flow of a thin rivulet on a vertical substrate subject to a prescribed uniform

shear stress at its free surface," *Physics of Fluids*, vol. 17, no. 10, Article ID 108105, 2005.

[51] J. P. Pascal and S. J. D. D'Alessio, "Instability of power-law fluid flows down an incline subjected to wind stress," *Applied Mathematical Modelling*, vol. 31, no. 7, pp. 1229–1248, 2007.

[52] S. K. Kalpathy, L. F. Francis, and S. Kumar, "Shear-induced suppression of rupture in two-layer thin liquid films," *Journal of Colloid and Interface Science*, vol. 348, no. 1, pp. 271–279, 2010.

[53] M. J. Davis, M. B. Gratton, and S. H. Davis, "Suppressing van der Waals driven rupture through shear," *Journal of Fluid Mechanics*, vol. 661, pp. 522–529, 2010.

[54] G. W. Sutton and A. Sherman, *Engineering Magnetohydrodynamics*, McGraw-Hill, New York, NY, USA, 1965.

[55] S. Kakac, R. K. Shah, and W. Aung, *Handbook of Single-Phase Heat Transfer*, John Wiley & Sons, New York, NY, USA, 1987.

[56] S. P. Lin, "Finite amplitude side-band stability of a viscous film," *Journal of Fluid Mechanics*, vol. 63, no. 3, pp. 417–429, 1974.

[57] M. V. G. Krishna and S. P. Lin, "Nonlinear stability of a viscous film with respect to three-dimensional side-band disturbances," *Physics of Fluids*, vol. 20, no. 7, pp. 1039–1044, 1977.

[58] B. Gjevik, "Occurrence of finite-amplitude surface waves on falling liquid films," *Physics of Fluids*, vol. 13, no. 8, pp. 1918–1925, 1970.

[59] H.-C. Chang, "Onset of nonlinear waves on falling films," *Physics of Fluids A*, vol. 1, no. 8, pp. 1314–1327, 1989.

[60] J. T. Stuart and R. C. DiPrima, "The Eckhaus and Benjamin-Feir resonance mechanisms," *Proceedings of the Royal Society of London A*, vol. 362, no. 1708, pp. 27–41, 1978.

[61] C. Godrèche and P. Manneville, *Hydrodynamics and Nonlinear Instabilities*, Cambridge University Press, New York, NY, USA, 1998.

[62] O. Gottlieb and A. Oron, "Stability and bifurcations of parametrically excited thin liquid films," *International Journal of Bifurcation and Chaos in Applied Sciences and Engineering*, vol. 14, no. 12, pp. 4117–4141, 2004.

[63] D. Armbruster, J. Guckenheimer, and P. Holmes, "Heteroclinic cycles and modulated travelling waves in systems with O(2) symmetry," *Physica D*, vol. 29, no. 3, pp. 257–282, 1988.

[64] J. Mizushima and K. Fujimura, "Higher harmonic resonance of two-dimensional disturbances in Rayleigh-Bénard convection," *Journal of Fluid Mechanics*, vol. 234, pp. 651–667, 1992.

[65] A. Samanta, "Stability of liquid film falling down a vertical non-uniformly heated wall," *Physica D*, vol. 237, no. 20, pp. 2587–2598, 2008.

[66] M. K. Smith, "The mechanism for the long-wave instability in thin liquid films," *Journal of Fluid Mechanics*, vol. 217, pp. 469–485, 1990.